AD-A044 624 AIR FORCE INST OF TECH WRIGHT-PATTERSON AFB OHIO F/G 6/18
RADIATION DOSE TO HUMANS FROM 99M TC LABELED DIHYDROTHIOCTIC AC--ETC(U)
1976 K N VANEK

UNCLASSIFIED AFIT-CI-77-14 NL

1 OF 2
AD A044624

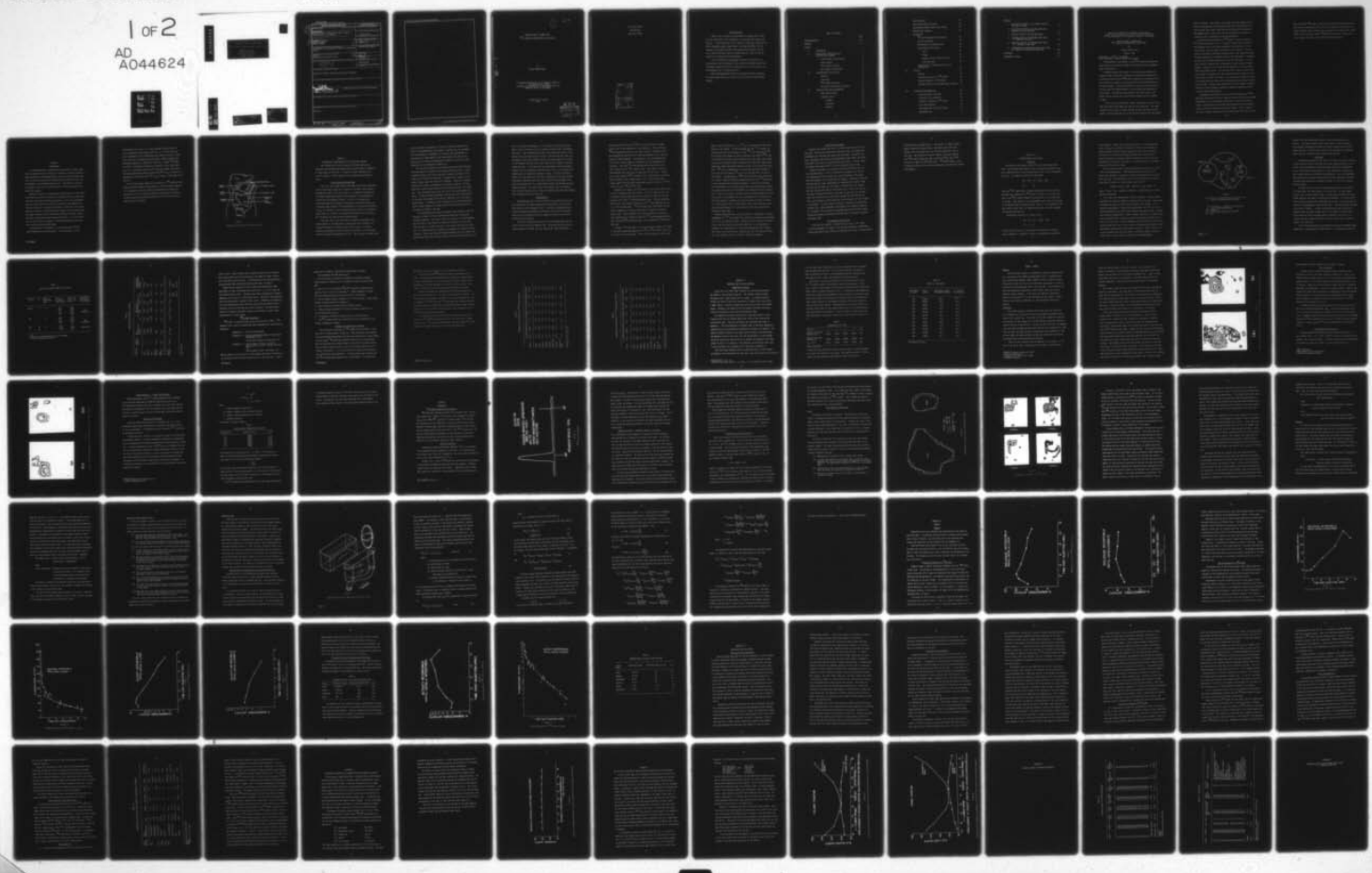

UNCLASSIFIED

SECURITY CLASSIFICATION OF THIS PAGE *(When Data Entered)*

REPORT DOCUMENTATION PAGE

READ INSTRUCTIONS BEFORE COMPLETING FORM

1. REPORT NUMBER: CI 77-14
2. GOVT ACCESSION NO.
3. RECIPIENT'S CATALOG NUMBER

4. TITLE *(and Subtitle)*: Radiation Dose to Humans From 99m Tc Labeled Dihydrothioctic Acid (DHTA),
5. TYPE OF REPORT & PERIOD COVERED: Dissertation
6. PERFORMING ORG. REPORT NUMBER

7. AUTHOR(s): KENNETH N. VANEK, CAPTAIN, USAF
8. CONTRACT OR GRANT NUMBER(s): Doctoral Thesis

9. PERFORMING ORGANIZATION NAME AND ADDRESS: AFIT Student at University of Florida, Gainesville, Florida
10. PROGRAM ELEMENT, PROJECT, TASK AREA & WORK UNIT NUMBERS

11. CONTROLLING OFFICE NAME AND ADDRESS: AFIT/CI, Wright-Patterson AFB OH 45433
12. REPORT DATE: 1976
13. NUMBER OF PAGES: 118 pages

14. MONITORING AGENCY NAME & ADDRESS *(if different from Controlling Office)*: 134 p.
15. SECURITY CLASS. *(of this report)*: Unclassified
15a. DECLASSIFICATION/DOWNGRADING SCHEDULE

16. DISTRIBUTION STATEMENT *(of this Report)*

Approved for Public Release; Distribution Unlimited

17. DISTRIBUTION STATEMENT *(of the abstract entered in Block 20, if different from Report)*

18. SUPPLEMENTARY NOTES

JERRAL F. GUESS, Captain, USAF
Director of Information, AFIT

APPROVED FOR PUBLIC RELEASE AFR 190-17

19. KEY WORDS *(Continue on reverse side if necessary and identify by block number)*

20. ABSTRACT *(Continue on reverse side if necessary and identify by block number)*

Attached

DD FORM 1 JAN 73 1473 EDITION OF 1 NOV 65 IS OBSOLETE

012200

UNCLASSIFIED

SECURITY CLASSIFICATION OF THIS PAGE *(When Data Entered)*

(1)

77-14

RADIATION DOSE TO HUMANS FROM ^{99m}Tc LABELED DIHYDROTHIOCTIC ACID (DHTA)

By

KENNETH NORMAN VANEK

A DISSERTATION PRESENTED TO THE GRADUATE COUNCIL OF
THE UNIVERSITY OF FLORIDA
IN PARTIAL FULFILLMENT OF THE REQUIREMENTS FOR THE
DEGREE OF DOCTOR OF PHILOSOPHY

UNIVERSITY OF FLORIDA
1976

To my wife Sheila

and children

Adam and Tiffany

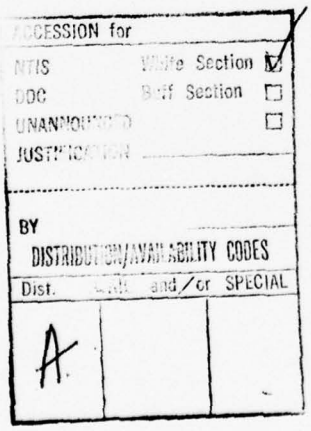

ACKNOWLEDGEMENTS

I would like to express my appreciation to everyone who, during the last three years, has assisted me in my personal and academic endeavors. I would especially like to thank my supervisory committee for their continued support, Penny Butler for nurturing MIRD#S, the 3M Company for providing the DHTA, the Gainesville VA Hospital for the use of their facilities, and the United States Air Force for the opportunity to continue my formal education.

I find it impossible to adequately express my gratitude to my chairperson, Valerie Brockeman for her scholarly guidance, advice, and invaluable support and to Larry Fitzgerald for all the assistance and encouragement that I received from him.

These acknowledgements would not be complete without expressing my utmost appreciation to my family for their love and understanding support.

TABLE OF CONTENTS

APPENDIX

Abstract of Dissertation Presented to the Graduate
Council of the University of Florida in Partial Fulfillment
of the Requirements for the Degree of Doctor of Philosophy

^{99m}Tc RADIATION DOSE TO HUMANS FROM ^{99m}Tc LABELED DIHYDROTHIOCTIC ACID (DHTA)

By

Kenneth Norman Vanek

August, 1976

Chairperson: Valerie A. Brookeman
Major Department: Nuclear Engineering Sciences

Dihydrothioctic acid (DHTA) is a new ^{99m}Tc-labeled hepatobiliary imaging agent for liver/gall bladder visualization and for diagnosing acute cholecystitis.

Nineteen patients with normal liver function were denied oral intake of food or drink after midnight and injected intravenously the following morning with 4mCi ^{99m}Tc-DHTA, prepared from a commercial kit. Each patient was scanned in a supine position from the mid-thoracic to mid-thigh regions. Scans were performed at various times from 0.25 to 12 hours after DHTA administration; 3 to 10 scans being recorded for each patient. The patients were allowed to eat fatty meals at the normal noon and evening meal times thereby inducing the gall bladder to empty.

A dual five-inch rectilinear scanner interfaced to a PDP-8/I computer with 16K of core memory was used for data collection. Data were recorded as the number of counts detected by each probe over a 6.35mm segment. Scanner speed was set so the area of interest could be scanned

within 15 minutes. New concepts and methods for organ boundary definitions and compensation for overlapping organs were developed and utilized to obtain the counts within each source organ for each detector. The geometric mean of the counts from the two detectors was then calculated for use in cumulated activity determinations.

The biological distribution of ^{99m}Tc-DHTA is similar to that of ^{131}I-sodium rose bengal since it is rapidly cleared from the blood by the polygonal cells of the liver and enters the intestines via the biliary tract with the kidneys excreting a small quantity. This biological distribution complicates determination of the quantitative data in humans necessary for absorbed radiation dose estimates, as evidenced by the lack of published quantitative data for rose bengal. In the normal patient, radioactivity concentration in the liver/gall bladder reaches a maximum of 15% of that injected between 2 to 4 hours after ^{99m}Tc-DHTA administration. The fatty noon meal induces the gall bladder to empty its contents into the intestines where the activity accumulates until excreted in the feces. The activity was assumed to remain in the intestinal area after the last datum point and decrease by physical decay only. Radioactivity concentration in the kidneys fluctuated around 4% of that injected, reaching its highest concentration about 1.5 hours after administration.

Cumulated activity ($\tilde{A}$) values for complete elimination of ^{99m}Tc-DHTA were determined utilizing a computer program which performs graphic integration of the experimentally determined acitivity distribution curves. Elimination after the last measured datum point was extrapolated to infinity assuming solely physical decay. Mean $\tilde{A}$ values for the liver, kidneys, intestinal area and blood were 1273, 352, 822, and

2002 μCi-hrs/mCi ^{99m}Tc-DHTA. Using recently published tables of absorbed dose per unit cumulated activity (S) and its property of additivity, absorbed radiation dose estimates were calculated to be 0.066, 0.079, 0.015, 0.004, 0.013, and 0.053 rads/mCi ^{99m}Tc-DHTA to the liver, kidneys, ovaries, testes, red marrow, and intestinal area respectively.

CHAPTER I

INTRODUCTION

In a 1969 symposium on radiation doses and effects, Smith stated that "the greatest single limitation in computing reliable estimates of absorbed dose from radiopharmaceuticals used in clinical nuclear medicine is the lack of data on the radionuclide distribution in man" (1). Unfortunately, this statement remains true. One reason for the lack of progress in this area is the difficulty in obtaining quantitative human data in vivo.

Dosimetric studies of hepatobiliary imaging agents and other radiopharmaceuticals which pass through the intestines possess unique problems which complicate obtaining in vivo data. First, the radiopharmaceutical is very mobile and thus many organs and organ segments are involved [Figure 1]. The area to be imaged is large and in most cases cannot be covered by a single stationary detector with one positioning. The organs involved are for the most part flexible and often overlap each other, complicating organ boundary definition. It is also difficult in these studies to develop a representative phantom and to provide accurate background subtraction.

Dihydrothioctic acid [DHTA] is a new technetium-99m [^{99m}Tc] labeled hepatobiliary imaging agent.* It has undergone clinical

*3M Company

investigations for use as a liver/gall bladder scanning agent (2) and for diagnosing acute cholecystitis (3 - 5). It has proven to be of additional value in identifying focal defects in sulfur colloid liver scans due to intrahepatic gallbladders, thereby avoiding the erroneous diagnosis of a metastatic lesion (2). Because ^{99m}Tc-DHTA is similar in biological clearance to iodine-131 [^{131}I] rose bengal (6), it is a potential agent for liver function studies, and, due to the higher administered doses possible with ^{99m}Tc [$T_{1/2}$= 6 hours] as a radionuclide label rather than ^{131}I [$T_{1/2}$= 8 days], it may prove to be superior.

With the forthcoming commercial availability of ^{99m}Tc-DHTA and subsequent increased number of applications in clinical nuclear medicine, it is necessary to know the radiation absorbed dose to humans concomitant with its use, thereby allowing the approrpiate decisions to be made concerning administered dosage and the risk versus benefit aspects of its utilization.

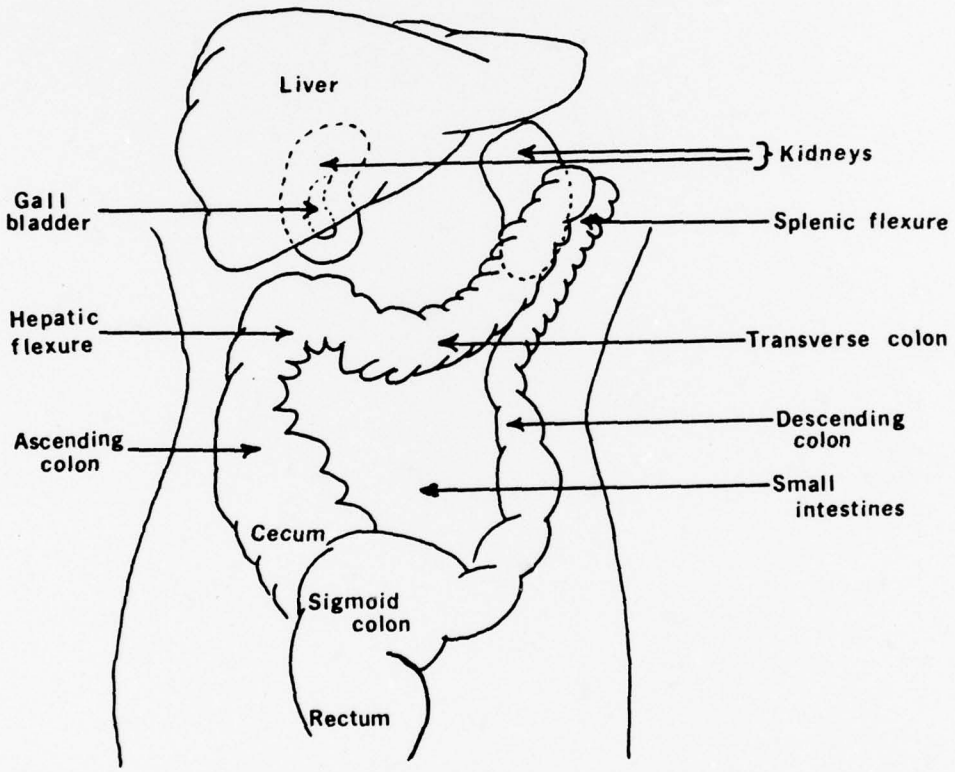

FIGURE 1.

Diagrammatic locations of pertinent organs.

CHAPTER II

RADIOISOTOPE INVESTIGATION OF LIVER AND GALL BLADDER

The information on liver structure or function that may be obtained with radiocompounds depends upon the physiological treatment of those agents by the liver. In order to better understand this area of interest, a brief review of liver anatomy and physiology is given.

Liver Anatomy and Physiology

The liver, the largest organ in the body, weighs about 1500 grams in the normal adult (7-9) and is located in the upper right quadrant. Although the shape of the liver varies, it is generally considered to be a wedge-shaped organ molded to the underside of the diaphragm and resting upon the abdominal viscera. The liver is strategically positioned between the intestinal and general circulation thereby providing the ideal location for the performance of its multiple functions. It has, for instance, a major influence upon the volume of circulating blood, acts as a "filter" of the materials absorbed by the intestine, and influences the water and electrolyte balance.

Sixty per cent of the liver mass is composed of polygonal cells [often refered to as hepatocytes or parenchymal cells] arranged in a sponge-like network of plates usually one cell thick. The plates branch and anastomose to form an intricate labyrinth of cells throughout which sinusoids interpenetrate (8, 9). The resultant sinusoids which

provide a tortuous passageway for blood are lined with Kupffer cells of the reticuloendothelial system [RES]. Kupffer cells are concerned with the breakdown of hemoglobin to bilirubin; they participate in the formation of gamma-globulin and immune bodies; and they act as scavenger cells removing by phagocytosis pigments, bacteria and other corpuscular or macromolecular elements (7).

The versatile polygonal cells perform many diversified functions including those of an endocrine and exocrine secretory nature. Since a detailed review of all their functions is beyond the scope of this study, only a few will be mentioned. Polygonal cells serve as a temporary storage center for many vital substances. Among their storage inventory are lipids, carbohydrates, and certain vitamins. The polygonal cells remove excess glucose from the blood and store it as glycogen. They also remove amino acids and "build" them into storable proteins. By removing these substances from the blood and releasing them as required, the polygonal cells play an important role in the body's energy supply. In addition, these remarkable cells perform detoxification of certain deleterious products that are either absorbed by the intestines or formed in the body.

The anastomosing thin plate arrangement of the polygonal cells is necessary in order for them to perform both endocrine and exocrine secretory functions. One side of the cell must abut on a blood passageway into which it can release its endocrine secretion, and the other side must abut on a lumen into which it can deliver the exocrine secretion. As indicated earlier, between the polygonal cell plates are blood sinusoids. Within the plates but between adjacent cells are spaces into which drains about 500 to 1000 ml per day of the exocrine secretion, bile.

Bile is secreted from polygonal cells into the bile canaliculus which makes its way along rows of cells eventually draining into intralobular bile ducts. The intralobular bile ducts join either the right or left hepatic duct which then leaves the liver. After leaving the liver, the two hepatic ducts merge, therby becoming the common hepatic duct which in turn combines with the cystic duct from the gall bladder to form the common bile duct. The common bile duct then empties into the duodenum. Although bile is continuously secreted by the liver, no bile enters the duodenum when the stomach or duodenum is empty. The bile, therefore, builds up in the common bile duct and is directed into the gall bladder whose mucosa reabsorbs water and salts leaving the bile pigment, bile acid, and calcium salts in a concentrated solution and thereby relieving internal pressure. Once food enters the duodenum, bile is allowed to flow into the intestine with a total gall bladder evacuation time ranging from 15 minutes to several hours (7).

Imaging Agents

Radiocompounds used for liver imaging can be classified into two main categories: [1] those phagocytized by the Kupffer cells and [2] those taken up by the polygonal cells. Colloids are phagocytized and usually permanently retained by the Kupffer cells, while those agents taken up by the polygonal cells are generally excreted into the bile canaliculi and bile ducts.

The use of radioactive colloids for liver imaging began with the efforts of Root and his co-workers (10). Encouraged by earlier distribution studies of colloids (11, 12), Root et al. (10) investigated

the distribution of Gold-198 (^{198}Au) colloids in humans and their possible use in the treatment of liver neoplasms. They found that ^{198}Au concentrated heavily in the liver except for neoplasmic areas and suggested the possibility of detecting neoplasms in the liver by external counting methods. Stirrett et al. (13, 14) performed the first scans of human subjects to demonstrate liver metastases and abscesses. They used ^{131}I labeled human serum albumin which was later replaced by the ^{198}Au colloids (15). Since then a variety of radiocompounds have been used to image the liver RES cells. Harper et al. (16) introduced ^{99m}Tc labeled sulfur colloid which is currently the most popular liver imaging agent in use. Other Kupffer cell imaging agents that have been investigated include Indium-113m [^{113m}In] colloid (17, 18), ^{64}Cu and ^{67}Cu (19).

Polygonal cell agents for scintigraphic liver imaging actually had an earlier beginning than the colloids. The first image of the liver by external radionuclide scanning was obtained in 1953 utilizing the polygonal cell agent ^{131}I-diiodofulorescein (20). Shortly thereafter, Taplin et al. (21) tagged rose bengal with ^{131}I and suggested its use as a liver scanning agent. ^{131}I-rose bengal has since become the most popular polygonal cell agent and has been the subject of numerous reports (22). Other polygonal cell imaging agents which have been investigated but not extensively used are ^{131}I-tetraiodophenolphthalein (23), Zinc-69m [^{69m}Zn]-chloride (24), and molybdenum-99m [^{99}Mo] molybdate (25).

Although ^{131}I-rose bengal is the most popular polygonal cell agent, it has never gained the popularity of ^{198}Au or ^{99m}Tc sulfur colloid in the study of liver morphology. There are many reasons for this, some

based on the limitations of using ^{131}I as a tag and some on the distribution of rose bengal. The 364 keV gamma ray from ^{131}I is harder to collimate than the 140 keV gamma ray from ^{99m}Tc and consequently ^{131}I will usually yield images of poorer resolution than those of ^{99m}Tc due to the greater collimator septal penetration of the higher energy gamma rays and to the greater amount of scatter both within the object being imaged and within the NaI[Tl] detecting crystal of the recording instrument. ^{99m}Tc can be administered in millicurie quantities because of its 6 hour half-life while ^{131}I, with an 8 day half-life, is given in microcuries. The gamma decay of ^{99m}Tc and its shorter half-life result in a smaller internal radiation absorbed dose than from ^{131}I which has a large non-penetrating radiation component. Colloids are desirable for scintigraphic liver imaging because not only have physicians become accustomed to the RES cell distribution for diagnosing certain diseases but, in the case of severe cirrhosis, large functional defects which may not be seen on a polygonal cell scan are apparent on the colloid scan. Since rose bengal is excreted into the bile canaliculi and bile ducts, it is also possible that a filling defect within the liver may be completely missed because it is transvered by a bile duct carrying the radioactive agent (26).

Recently there has been an active interest in developing a suitable replacement for ^{131}I-rose bengal (2-6, 27-35) to eliminate the objections to ^{131}I as the radioactive label. Because of their biological distributions, these new agents should prove beneficial in the assessment of polygonal cell function and in identifying intrahepatic gall bladders and biliary tract obstructions. Although they will not replace colloids for liver scanning, they will provide a valuable supplement.

Liver Function Studies

Unlabeled rose bengal was used in liver function tests as early as 1923 (36). These early studies used colorimetric means to measure the disappearance of injected rose bengal from the blood. Gradually, however, rose bengal was replaced by bromosulfalein (BSP) which, not being colorimetric, was not as easily affected by bilirubin. In 1955, Taplin (21), tagged rose bengal with ^{131}I and its popularity was revived.

Because rose bengal is extracted from the blood primarily by the liver [approximately 1 to 2% is cleared by the kidneys], the rate of its disappearance from the blood can be used to measure liver blood flow and polygonal cell function (22, 26, 37-39). Clearance of colloids from the blood has been investigated for measurement of hepatic blood flow (22, 26) but their use is limited. Patients with liver disease may have reduced efficiency of the Kupffer cells in the liver but significantly increased efficiency of the RES in other parts of the body. Since the colloids are not then solely removed from the blood by the liver, the estimate of liver blood flow in the presence of liver disease is unreliable. In those cases of hepatitis, cirrhosis, or obstructive jaundice [i.e. severe impairment of polygonal cell function] clearance of rose bengal from the blood is prolonged whereas RES function remains undisturbed thereby enforcing the unreliability of colloidal clearance techniques (40).

Gall Bladder Visualization

Since the gall bladder is routinely visualized in liver scans utilizing polygonal cell agents, this may have diagnostic significance. Patton (26) reports gall bladder visualization when there is cholecystitis,

cholelithiasis, pancreatic disease, and partial or complete extra-hepatic obstruction (though not at the hepatic duct level) and believes that rose bengal does not offer any diagnostic value in this area. More optimistic results, however, have been reported with ^{99m}Tc-penicillamine (41, 42), gallium-67 [^{67}Ga] (43), ^{99m}Tc-tetracycline (44), and ^{99m}Tc-DHTA (2-5). ^{99m}Tc-DHTA appears to have a promising future for this clinical application and should be further investigated.

CHAPTER III

DIHYDROTHIOCTIC ACID (DHTA)

Chemistry

The chemical nomenclature of DHTA is DL 6-8 dimercaptooctanoic acid. Some synonyms which appear in the literature are reduced lipoic acid, reduced thioctic acid, DL dihydrolipoic acid, and DL dimercaptolipoic acid. Its chemical structure is shown below.

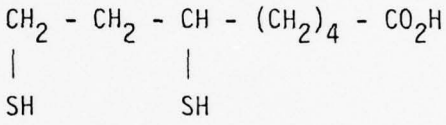

Since the ^{99m}Tc labeled form is newly developed and has not yet been marketed, the information on ^{99m}Tc-DHTA is limited. The actual structure of the ^{99m}Tc labeled compound resulting from its kit preparation is unknown. DHTA, however, is interchangeable with lipoic acid *in vivo* via oxidation-reduction reactions (45). Thus, it is of interest to discuss briefly lipoic acid, its reduced form (DHTA), and their apparent relationship and function.

The chemical structure of α-lipoic acid is

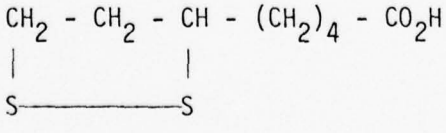

During the last 20 years, it has become recognized as a prosthetic group, coenzyme, or substrate in plants, microorganisms, and animal

tissue (45-47). Because of its coenzyme function, it was thought that lipoic acid may be an essential vitamin, but there is no evidence currently available which will either support or reject this assumption. The difficulty in obtaining necessary evidence arises from the fact that the substance is not only widely distributed in food, but is also synthesized by intestinal flora (45). A lipoic-free diet, is therefore, extremely difficult to maintain.

The only enzymes known to contain protein-bound lipoic acid are the α-keto acid dehydrogenases. These enzymes mediate the formation of energy-rich coenzyme A compounds by oxidative decarboxylation of α-keto acids (45, 46). The physiological function of the enzymes can thus be described as catalysis of the following reaction (45):

$$RCOCOOH + HS\text{-}CoA + NAD^+ \rightarrow RCO\text{-}S\text{-}CoA + CO_2 + NADH + H^+$$

where R = alkyl, CoA = coenzyme A, NAD/NADH = oxidized/reduced nicotine adenine dinucleotide.

The α-keto acid dehydrogenases actually represent multiple enzyme complexes with molecular weights of several million (47, 48). Three types of enzymes have been isolated from the complexes (47, 49-52): [1] A thiamine pyrophosphate - containing decarboxylase, [2] a lipoic acid reductase transcylase, and [3] a flavin adenine dinucleotide [FAD] - containing lipoamide oxidoreductase. These 3 enzymes function as a transfer mechanism transferring the α-keto acids derived from glucose metabolism into the citric acid cycle. A model frequently used to explain the function of protein-bound lipoic acid in the α-keto acid dehydrogenase complex is that developed by Reed (53) and illustrated in Figure 2. Lipoic acid acts as an acyl acceptor where the acyl group is exclusively bound to the C-6 sulfur atom. The acyl group is picked from the dehydrogenase

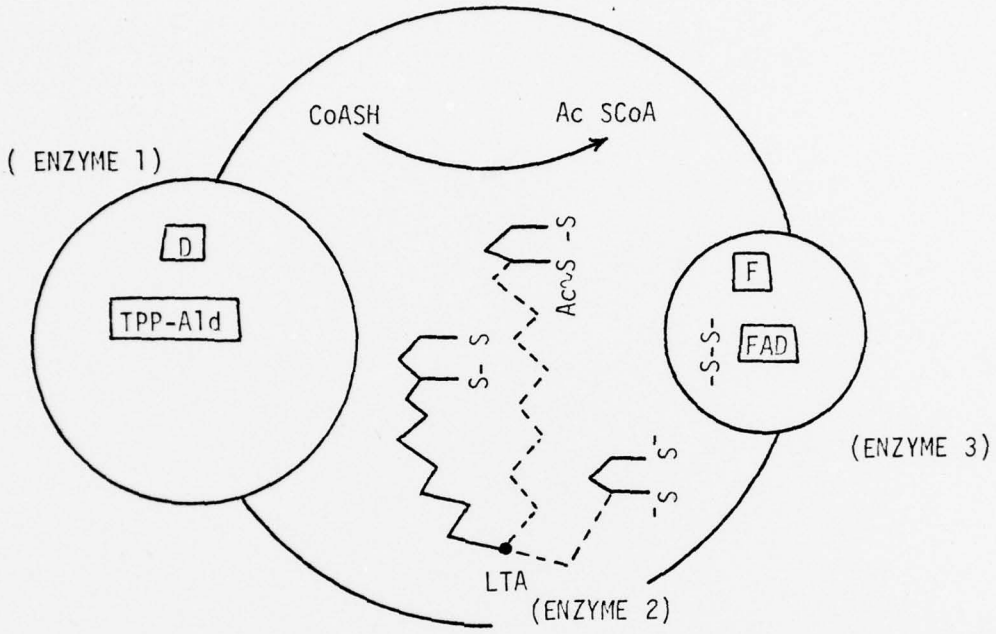

FIGURE 2.

The function of protein-bound lipoic acid in the α-keto acid dehydrogenase complex*.

F = flavoprotein = lipoamide oxidoreductase.
D = α-keto acid decarboxylase.
CoA = coenzyme A
LTA = lipoic acid reductase transacylase
Ac = acyl

*(53)

[Enzyme 1] by the transacylase [Enzyme 2] and then transfered to co-enzyme A. The reduced protein-bound lipoyl moiety is then oxidized by the lipoamide oxidoreductase [Enzyme 3] thereby regenerating the second enzyme (45, 53). A more detailed review of the biochemistry of DHTA and lipoic acid may be found in the literature (45, 48, 54).

Toxicology

A threefold evaluation of the toxicity of DHTA consisting of studies on acute toxicity, local irritation, and 21-day subacute toxicity is presented in the Investigation of New Drug Report 9567 (6) and summarized below. Riker Research Laboratories, St. Paul, Minnesota, performed the acute toxicity and local irritation investigations. They also determined the concentrations and doses that were used by the International Research and Development Corporation, Mattawan, Michigan, in the 21-day subacute toxicity studies.

The acute toxicity tests utilized DHTA preparation kits containing 51.7 mg/ml DHTA, 28.1 mg/ml $NaHCO_3$, 0.472 mg/ml Sn^{II}, 9.0 mg/ml benzyl alcohol, and 15.7 mg/ml ethyl alcohol. Animals were purchased from established suppliers and housed in controlled environments. For several hours after injection and then daily thereafter for 14 days, the animals were observed for pharmacodynamic signs and mortality. The mortality data obtained are outlined in TABLE 1. Further investigation with dogs established a minimum lethal dose (MLD) greater than 13.2 mg DHTA per kg body weight. Toxic doses were noted to produce local irritation at the site of injection, anorexia, depression, emesis, ataxia, bloody stools, diarrhea, tremors, and convulsions.

Local irritation analysis was performed using male New Zealand white rabbits and 5 concentrations of DHTA [TABLE 2]. Injections were made via

TABLE 1

DHTA ACUTE TOXICITY MORTALITY STUDIES*

Species	Sex	Mode of Administration	Dose of mg DHTA/kg body weight	14 day cumulative mortality	LD50 Results mg DHTA/kg body weight
Mouse	M	iv	229	6/10	
			204	5/10	
			182	2/10	210
			162	0/10	(195-227)
			145	0/10	
Rat	F	iv	262	8/10	
			234	8/10	
			209	4/10	226
			186	0/9	(215-238)
Dog	M	iv	155.1	1/1	
	F		103.4	2/2**	MLD***51.7
	M		51.7	2/2	

* (6)
** one dog was euthanized because of distemper
*** MLD = minimum lethal dose

TABLE 2

IRRITATION AND SUBACUTE STUDIES*

Component	Control (mg/ml)	Use Concentration (mg/ml)	Multiples of Use Concentration (mg/ml) 5X	10X	20X	120X	Supplemental Concentration (mg/ml)
DHTA	- - -	0.445	2.23	4.45	8.90	51.7	0.443
$NaHCO_3$	- - -	0.974	4.87	9.74	19.5	128.1	0.99
Snll	- - -	0.00392	0.0196	0.0392	0.0784	0.472	4.18
Benzyl Alcohol	9.00	9.00	9.00	9.00	9.00	9.00	9.20
Ehtyl Alcohol	8.67	8.67	8.67	8.67	8.67	8.67	8.47
Amount Injected	5 ml/kg	not used	5 ml/kg	5 ml/kg	5 ml/kg	73 mg DHTA per kg	0.625 mg DHTA per kg

*(6) modified

the ear veins. Results showed that intravenous doses up to 44 mg DHTA per kg body weight were non-irritating to the rabbit ear when a volume of 5 ml/mg body weight was used. An intravenous dose of 260 mg DHTA per kg body weight [same volume] did produce some local irritation.

Twenty-one day subacute toxicity studies were performed on dogs and rabbits divided into groups each receiving 0, 1, 3, or 10 times the use concentration of DHTA. Injections were made intravenously on Monday, Wednesday, and Friday for 3 consecutive weeks. The animals were observed daily and body weights recorded 3 times a week. Hematology, biochemistry, and urine determinations were made once during the pre-injection period and again at the 7th and 21st day of post-injection. No drug related gross or microscopic pathologic lesions or variations in organ weight were observed in these studies.

^{99m}Tc-DHTA Preparation

^{99m}Tc-DHTA is prepared simply using the eluate from a ^{99}Mo - ^{99m}Tc generator and a sterile, pyrogen-free three component kit* containing the following:

Container A --- 2.0 ul [2.27 mg] DHTA

Container B --- 4.91 mg sodium bicarbonate, United States Pharmacopeia [USP]

1.0 ml sterile water for injection, USP

Container C --- 38 ug stannous chloride, dihydrate
45.9 mg benzyl alcohol, National Formulary [NF]

44.2 mg ethyl alcohol, 200 proof, USP

Quality control specifications* for DHTA require that 80% of the DHTA be in the dihydro form with the remainder being in the disulfide. Current

*3M Company

production is, however, yielding 95% dihydrolipoic acid (55).

The procedures for DHTA labeling are

1. Add the contents of container B [$NaHCO_3$] to container A [DHTA]. Shake container A vigorously for 30 seconds to insure solution of the DHTA.
2. Add 2.0 to 4.0 ml of $NaTcO_4$ [^{99}Mo-^{99m}Tc generator eluate] with an activity from 1 to 10 mCi to container A. Invert container A several times for proper mixing [10 mCi was utilized in this study].
3. With an unused syringe, withdraw 0.10 ml from container C [$SnCl_2.2H_2O$/ ethanol solution] and add to container A.
4. Invert container A several times for proper mixing.
5. Allow the drug [container A] to stand at ambient conditions for 15-20 minutes before using.
6. If necessary, dilute with normal saline to desired activity.
7. The ^{99m}Tc labeled DHTA may be checked for free pertechnetate using various chromographic methods.

Biological Distribution in Animals

The biological distribution of ^{99m}Tc-DHTA has been studied in mice (6) and to a limited extent in dogs (3). Forty-two female Swiss Webster mice each weighing approximately 20 grams were divided into 6 equal groups. For each group, ^{99m}Tc-DHTA was prepared according to the instructions with the labeling kit and then diluted to 4 uCi/ml with isotonic saline. The mice were injected iv with 0.1 ml of the diluted solution and at 5 minutes, 30 minutes, 1, 2, 4, 6 and 24 hours an animal from each group was sacrificed by CO_2 asphyxiation. The major organs were isolated and the ^{99m}Tc concentration measured with a spectrometer. The results for

*3M Company

each time interval were averaged and are presented in TABLE 3.

It can be seen that ^{99m}Tc-DHTA was rapidly concentrated in the liver. The liver activity decreased with a half-time of approximately 0.7 hours (6) and after 1 hour the majority was either located in the intestines or had been excreted in the urine and feces (mostly in the feces). Almost 96% of the activity had been excreted by 24 hours.

The above experiment was repeated using ^{131}I-rose bengal* and 2 mice per time interval (6). The results are summarized in TABLE 4. It can be seen from a comparison of TABLES 3 and 4 that although the rates of transport for ^{99m}Tc-DHTA and ^{131}I-rose bengal are somewhat different the major routes of distribution are identical, namely, removal from the blood by the liver, transfer from the liver to the intestines via the biliary tract, and finally excretion.

The investigations utilizing dogs were performed by injecting iv 420 uCi of ^{99m}Tc-DHTA and imaging over the liver region with a gamma camera (3, 6). The same major distribution route was noted with a well defined gall bladder detected at 120 minutes post-injection.

*Abbott Laboratories

TABLE 3

BIOLOGICAL DISTRIBUTION OF ^{99m}Tc-DHTA IN MICE*

Source	% of Administered Dose at Different Times After Administration						
	5 min	30 min	1 hr	2 hr	4 hr	6 hr	24 hr
Lungs	1.3	0.7	0.5	0.3	0.1	0.0	0.0
Liver	62.9	45.4	27.4	11.8	6.3	4.5	1.6
Spleen	0.1	0.1	0.0	0.0	0.0	0.0	0.1
Kidneys	5.4	2.8	2.2	1.5	0.9	0.8	0.4
Stomach	0.4	0.4	0.3	0.7	0.3	0.6	0.1
Intestines	7.4	29.4	35.7	43.9	28.9	19.3	0.8
Carcass	21.0	9.8	6.8	4.4	1.5	1.3	1.2
Urine and Feces	1.5	11.4	27.1	37.4	62.0	73.5	95.8

*Average of six mice (6).

TABLE 4

BIOLOGICAL DISTRIBUTION OF ^{131}I-ROSE BENGAL IN MICE*

Source	% of Administered Dose at Different Times After Administration						
	5 min	30 min	1 hr	2 hr	4 hr	8 hr	24 hr
Lungs	2.9	0.6	0.4	0.3	0.3	0.2	0.1
Liver	60.0	22.6	13.1	7.4	5.0	5.0	3.8
Spleen	0.2	0.3	0.2	0.3	0.2	0.3	0.3
Kidneys	2.7	1.3	0.9	0.8	0.5	0.5	0.4
Stomach	0.9	3.2	4.9	1.0	8.9	0.2	0.5
Intestines	8.1	63.0	65.4	84.1	41.7	1.5	0.5
Carcass	25.2	8.7	13.0	3.6	3.6	1.9	0.6
Urine and Feces	0.0	0.3	2.1	2.5	37.3	90.4	93.8

*Average of two mice (6).

CHAPTER IV

MATERIALS AND THEIR CALIBRATION

Rectilinear Scanner

A dual five-inch rectilinear scanner* with focused collimators** was chosen as the radiation detector. The scanner offered multiple advantages over a gamma camera for this study. It proved to be both simpler and faster to scan the large area of interest than to position a gamma camera a minimum of three times and then correlate the recorded images. Moreover, the scanner with its focused collimators can essentially be considered a very large fixed detector (56).

The subject-to-detector distance has a negligible effect in area scanning when the scan extends beyond the limits of the radionuclide distribution (57). This was verified by the experiment described in Appendix 1. By using detectors on opposed sides of the body, geometrical considerations are minimized and attenuation variations are reduced. The effect of depth variation of an organ within the body is minimized when the geometric mean of the counts from the two detectors is used (56-59). Since the question has been raised as to whether the geometric mean alone should be used or the average of the geometric and arithmetic means (60), a short experiment was conducted and is described in Appendix 2.

With the kidney phantoms which are described later in this chapter, the geometric mean decreased less than 16% as the source center was displayed

*Ohio-Nuclear Series 84
**Ohio-Nuclear Model 55035-1, 163 holes, 12.7 cm geometric focal length

7 cm on either side of the center of the water bath while the arithmetic mean increased more than 52%. With the volume phantom, the geometric mean decreased 6% over the 7 cm displacement while the arithmetic mean increased over 35%. Hence, the geometric mean alone was used.

Uniformity of detector head speed was verified by attaching a 25 μCi ^{57}Co sealed source to the detector head and scanning over a small area. Counts in each element of the computer image [described below] were equal within 2 standard deviations [s.d.]. The gamma-ray spectrometer was checked for linearity and alignment of the two probes was assured by scanning a point source and verifying that the peak counts in both upper and lower images occurred in corresponding locations within the respective working areas of the computer. Repeatability of a scan was verified by scanning three times over the volume phantom with 3.8 cm pressed wood between the detectors and phantom. As seen in TABLE 5, counts within the organ boundaries, after decay correction, did not vary by more than $\pm$ 1.5 s.d.

TABLE 5

REPEATABILITY OF SCAN

Scan No.	1	2	3	$\bar{x}$	s.d.
Counts* from upper detector (u)	319416	319073	319991	319493	464
Counts* from lower detector (l)	308504	308080	308943	308509	482
$(u \times l)^{1/2}$	313913	313528	314418	313953	446

*decay corrected

A check was also performed to assure that the number of counts detected was linear with respect to scan speed. The results are shown in TABLE 6. Counts and scan speed were normalized to those at 100 cm/min.

TABLE 6

COUNTS VS. SCAN SPEED

Scan Speed (cm/min)	Total Counts*	$\frac{100 \text{ cm/min} \times 100\%}{\text{Scan Speed (cm/min)}}$	% of Counts at 100 cm/min
100	801945	100.0	100.0
125	638351	80.0	79.6
150	539682	67.0	67.3
200	408425	50.0	50.9
225	365056	44.4	45.5
250	327149	40.0	40.8
300	272977	33.3	34.0
350	233873	28.6	29.2
400	204338	25.0	25.5
450	182192	22.2	22.7
500	162680	20.0	20.3
600	135025	16.7	16.8

*Corrected for decay.

Computer System

Hardware

The rectilinear scanner is interfaced to a PDP-8/I computer* with 16 K core memory and an RF08 word-addressable disk.* A standard automatic send-receive teletype (model 33ASR)** is used to input or output information at the rate of up to ten characters per second or to read in or punch out perforated paper tape at the same rate. The system has two TU55 tape transports* operated by a TC01 control unit* and utilizes standard 10-track DECtape. A 132 column, 64 character, 4000 series (Model A) line printer *** is also available for data output. Visual display is provided by an HP1300A X-Y oscilloscope**** having a P_7 phosphor.

Interfaces

The scanner-computer interface (61) divides the scan lines into 0.25" segments and by using 0.25" line spacing each data element represents a 0.25" square area. The pulses in each data element are fed from each detector to the computer by a single interface using the program-interrupt facility of the PDP-8/I. The data are fed into Field 1 of magnetic core, the lower and upper 2K words being reserved for accumulation of data from the upper and lower detectors respectively, until another full line of data cannot be stored and then the data are transferred to the disk. Data images were stored permanently on DECtape.

There are two interfaces from the computer to the display. A VC-8/I* is for the x- and y- coordinates and the other, a 32 gray level

*Digital Equipment Corporation (DEC)
**Teletype Corporation
***Mohwak Data Sciences Corp. (MDS)
****Hewlett Packard

intensity interface (61), is for the z signal. During display, the image is smoothed by also displaying points which have been interpolated between the data points on a line and also between lines. Hence an image containing N data points is displayed as a 4N image thereby providing a smoother appearance. Numerical data are printed out by a line printer.

Software

The software system utilized was developed by Bell et al. (61-62) and operates in two modes. The lower mode is for data-acquisition and the upper mode for data-handling. The majority of the commands are nondestructive, operating only on data stored in core leaving the disk data intact. The normal display mode which occurs during data-handling has already been mentioned. In addition, there is a boustrophedonic display during data-access which displays each element as a point when it is acquired.

There are multiple data processing options available with this system, details of which will not be presented here. Some of these utilized in this study were count subtraction, averaging or smoothing with a gaussian matrix, and a coarse antiscatter and antipenetration correction. These options were used to enable definition of the localization of ^{99m}Tc-DHTA in each image. Without the use of such data-processing, identification of the organs in which the radiopharmaceutical had localized and organ boundary definitions would have been much more difficult as illustrated in Figure 3 which shows the effect of these data-processing routines. Both images had 40 counts subtracted from each data point but only Figure 3 B received further processing. Both images are also shown in the multicycle contrast enhancement display mode which permits a somewhat quantitative visual examination of the image. Basically, this display mode should be viewed as a radioactivity contour map. Processed images

(A) (B)

FIGURE 3.

Effect of scatter and smoothing corrections on image quality. (A) Uncorrected (B) Corrected

from the upper and lower probes are also shown in Figure 4.

Dose Calibrator

The Mark V dose calibrator* which was used to measure isotope activities utilizes a well-type ionization chamber [8 in. deep x 8 in. diameter] with a stated accuracy of ± 5% and long term reproduceability greater than 98%. The digital readout has an operating range of 1 μCi to 1000 mCi. Before an activity reading is made, the unit is zeroed to compensate for background. If too great a negative bias is applied, the display will flash until the setting is readjusted to the correct amount. Isotope selection is made by choosing the appropriate plug-in module which introduces a calibrated resistance into the system. The ^{99m}Tc module has a resistance of 102.7 KΩ.

A monthly calibration was performed using a 10.2 mgm radium standard and a variable potentiometer (63). With the potentiometer set at 11.2 KΩ, the dose calibrator was adjusted to read 10.2 on the 0-100 mCi scale. Biweekly calibration checks were performed utilizing a calibrated Cesium-137 (^{137}Cs) standard** (10.8 ± 5% mCi on 3/28/75), model NER-401H (serial no. CS213), and the ^{137}Cs plug-in module with a resistance of 24.6 KΩ.

Blood Sample Counting System

The Auto-Gamma*** spectrometer used to count blood samples is a well-counter with a 1.75 x 2.00 in. NaI(Tl) crystal, an automatic sample changer, and a print-out device. An energy calibration was performed and the system was found to be linear at a gain setting of 45.35.

*RADX Corporation
**New England Nuclear Corporation
***Packard Instrument Company

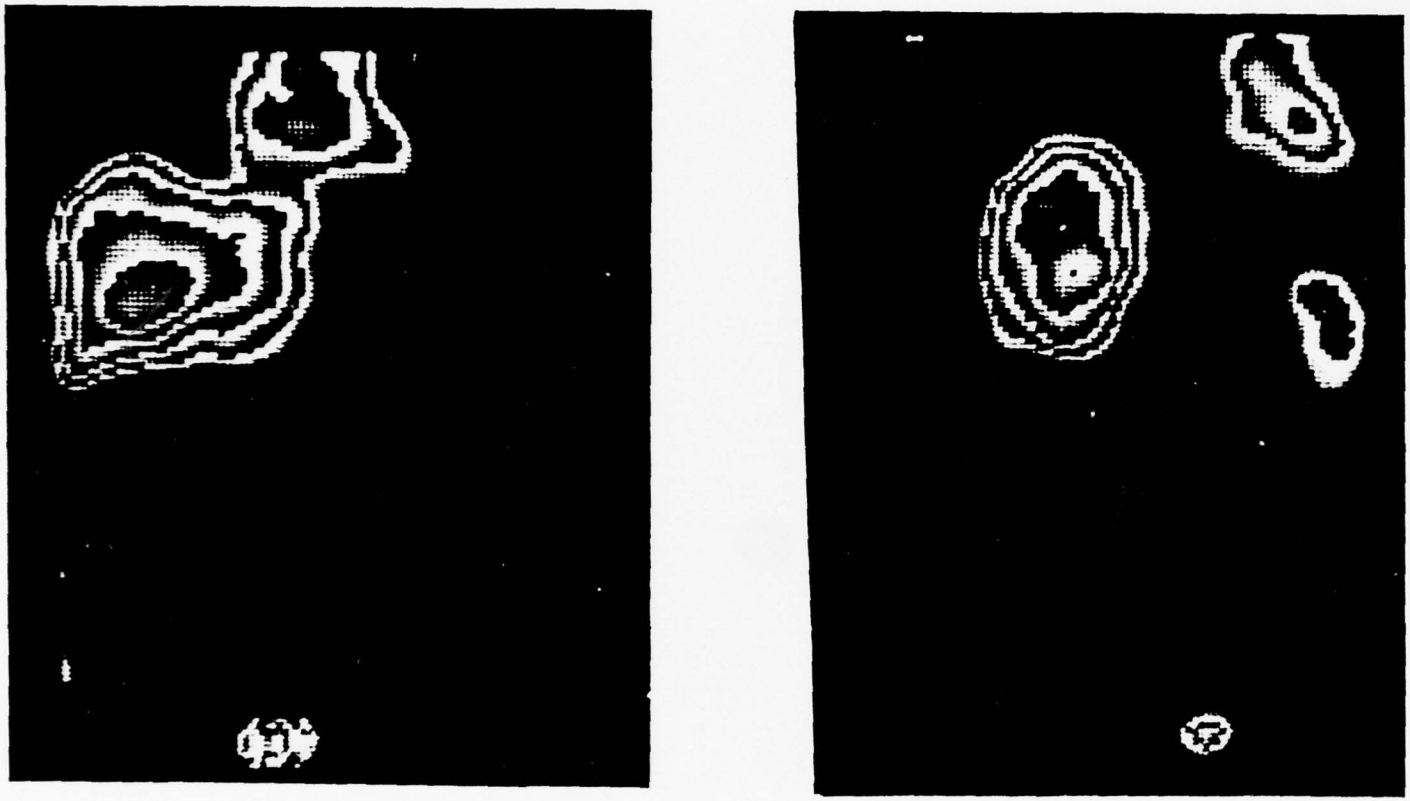

(A) (B)

FIGURE 4.

Comparison of views from scanner's (A) upper detector and (B) lower detector

Radiochromatographic Paper Strip Scanner

Radiochromatograms of the ^{99m}Tc-DHTA preparations were obtained using the system developed by Sunderland (64) which consists of a collimated Geiger-Mueller (GM) tube, ratemeter, and strip chart recorder. The prepared chromatography strip is attached to the chart paper and as the strip is pulled across the face of the GM tube, the activity distribution is recorded.

Phantoms and Standards

Liver and kidney phantoms* plus a rectangular (20 x 13 x 8 cm) plexiglass phantom which represented the intestinal area were utilized in this investigation. All phantoms could be filled with ^{99m}Tc solutions of appropriate activity.

Pressed wood (3.8 cm thick, 0.72 gm/cm^3) was used as the scattering and absorbing medium. Its linear attenuation coefficient was determined using a Pho/Gamma HP scintillation camera** with a high resolution collimator. A syringe containing 0.54 mCi of $Na^{99m}TcO_4$ was collimated with lead bricks and placed 44.5 cm from the pressed wood absorber and 122 cm from the face of the camera collimator. Varying thicknesses of pressed wood were placed between the source and detector and the counts per minute recorded by the scintillation camera were noted for each thickness. An attenuation coefficient (μ) was determined for each measurement using the equation for μ below.

*Alderson Reasearch Laboratories, Inc.
**Searle Radiographics Inc.

$$I = I_0 e^{-\mu x}$$

$$\ln (I/I_0) = -\mu x$$

$$\mu = -x \ln (I/I_0)$$

where

μ = linear attenuation coefficient

I_0 = number of photons with no absorber present

I = number of photons penetrating the absorber

x = absorber thickness

The results are shown in TABLE 7.

TABLE 7

PRESSED WOOD ATTENUATION COEFFICIENT

Thickness(cm)	Counts Per Min	$\mu(cm^{-1})$
0	72902	
1.9	59723	0.105
3.8	48625	0.107
5.7	40071	0.105
7.6	33129	0.104
9.5	26885	0.105
11.4	21889	0.105

The average of the values given for μ in TABLE 7 is 0.105 which is equal to that obtained using the experimetally determined half-value layer (HVL) of 6.6 cm and the following equation.

$$\mu = \frac{\ln 2}{HVL}$$

By using the linear attenuation coefficient for 140 KeV photons in water (0.153) it was determined that a 3.8 cm thickness of pressed wood was equivalent to 2.6 cm of soft tissue which is representative of the tissue thickness overlaying the liver.

Two ^{57}Co standards were prepared for use in the gamma spectrometer.

A calibrated aqueous solution of ^{57}Co [the stated activity was verified ty measurement in the dose calibrator] was diluted to an activity of 0.19 μCi/ml. Two samples 1.0 ml each were withdrawn with a micropipette. Both samples were then counted in the well-counter and were within 2 s.d.

CHAPTER V

METHODOLOGY

^{99m}Tc-DHTA Preparation and Analysis

^{99m}Tc-DHTA was prepared according to the manufacturer's instructions [described in Chapter III], using a three component kit and the eluate from a ^{99}Mo-^{99m}Tc generator* Binding between ^{99m}Tc and DHTA was determined for each preparation using an ascending paper chromatography technique (64), modified by employing acetone as the solvent, and was greater than 95% with less than 5% free ^{99m}Tc [Figure 5]. The activity administered intravenously to each patient was accurately determined by measuring the activity in the syringe employed with a RADX Mark V dose calibrator before and after injection.

Clinical Procedure

Nineteen male patient-volunteers [Appendix 3] with no suspected liver abnormalities were analyzed in this study. The average patient was 55 years old, 172 cm tall, weighed 67.1 kg, had a chest thickness of 23.4 cm and a waist thickness of 22.5 cm.

Around 8 A.M., 4 mCi of ^{99m}Tc-DHTA were administered intravenously to the patient-volunteers who had been NPO since midnight. Informed consent forms were signed by each subject. Immediately after voiding, each subject was scanned in a supine position from the mid-thoracic to

*E.R. Squibb & Sons, Inc.

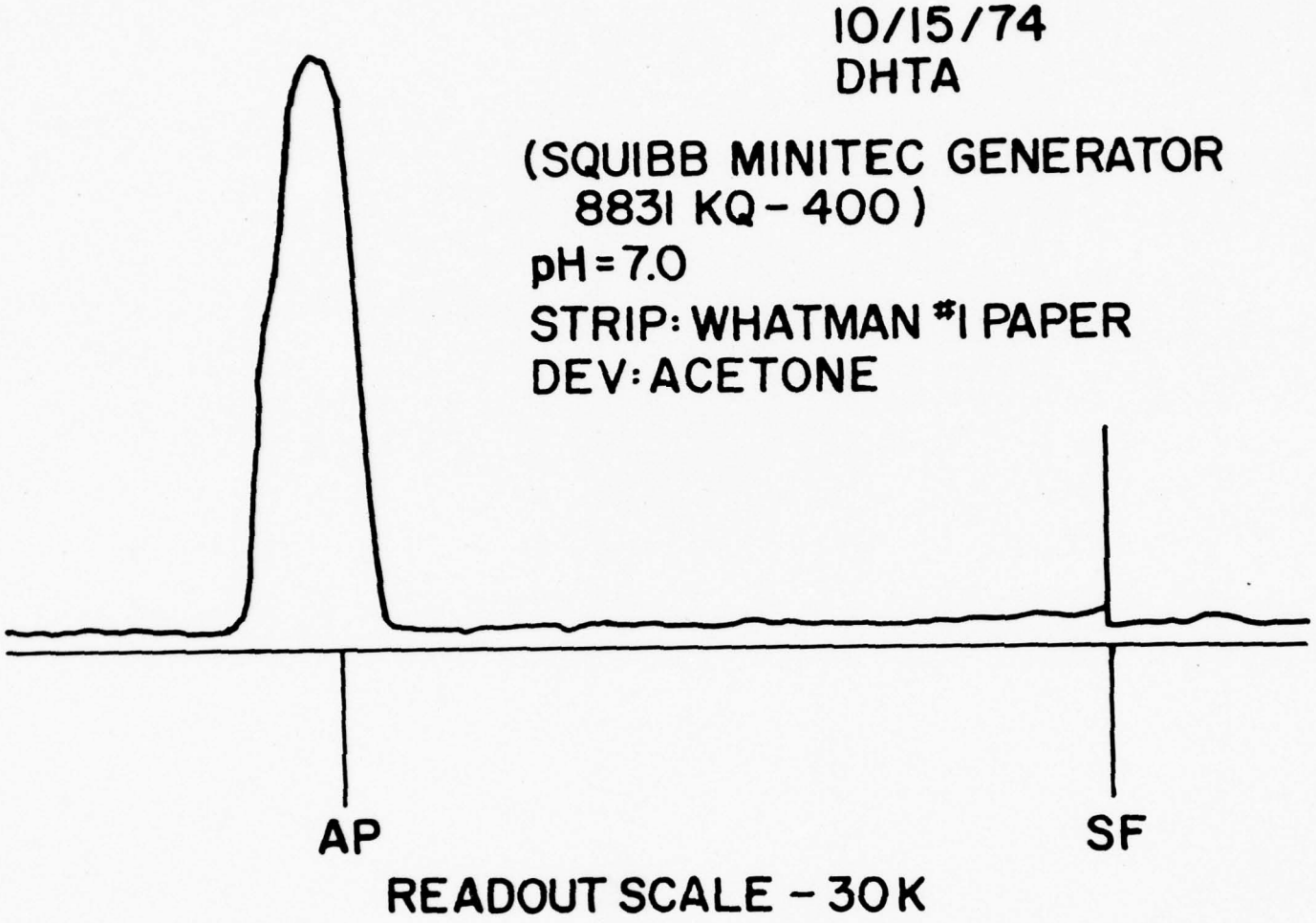

FIGURE 5.

^{99m}Tc-DHTA Chromatogram

mid-thigh regions. Scans were performed at various times from 0.25 to 12 hours after DHTA administration and 3 to 10 scans were recorded for each subject. A total of 133 scans were made of the 19 patients averaging 7 scans per patient. For each scan except two, scan speed was set at 250 cm/sec and longitudinal speed at 750 cm/sec thus allowing the area to be scanned in 15 minutes or less. With one patient, the scan speed was reduced to 225 cm/sec for the 10.4 and 11.5 hr images. Since the number of counts detected is linear with respect to scan speed [TABLE 6], it was possible to normalize the counts observed at 225 cm/sec to those that would be observed at 250 cm/sec using the following relationship:

NORMALIZED COUNTS = [OBSERVED COUNTS] x [225/250]

This normalization thus allowed all calculations to be performed on data obtained at or normalized to the same scan speed. For different patients, the distance of the upper detector to the top of the scan table varied from 26 to 31 cm with an average distance of 28.5 cm while the lower detector was positioned a constant 1.5 cm from the top of the scan table. Detector positioning was identical for each scan performed on a particular subject. The times at which the scans were recorded and the number of scans were dependent upon the subject's condition and hospital schedule and upon the nuclear medicine department's schedule. The subjects were allowed to eat fatty meals at the normal noon and evening meal times thereby inducing the gallbladder to empty.

For each study, phantoms containing a known amount of radioactivity were placed on the scanning table with 3.8 cm pressed wood between the detectors and the phantom. The activity placed in each phantom was accurately determined by measuring the activity in the syringe employed with the

dose calibrator before and after injection of the activity into the phantom. The amount of ^{99m}Tc placed into each phantom was variable but representative of the count rate observed in the associated human organ. The phantoms were then scanned at the same speed as the patient with the detectors at the same distance from the scan table.

Blood samples were obtained whenever possible by withdrawing 1.5 to 2.0 ml of blood with a 3 ml syringe and then transferring the blood to a 5 ml blood collecting tube containing 0.048 ml of 15% potassium ethylenediaminetetraacetic acid [EDTA] which served as the anticoagulant. A total of 30 blood samples were collected from 9 patients. Patient reluctance plus difficulty in obtaining some samples due to poor veins were limiting factors.

Determination of Blood Activity

1.00 ml was withdrawn from the blood sample with a micropipette and placed into a counting vial. The vial was then counted twice each for 1.0 min. Both ^{57}Co standards were also counted twice with each set of blood samples. The discriminator settings of the spectrometer were selected so that the single-channel window was 60 to 200 keV. The ^{57}Co standards counts, C [Co] were then related to ^{99m}Tc counts, C [Tc], by the following equation (65):

$$C\,[Tc] = 90/98\ C\,[Co]$$

where 90 represents the number of 140 keV photons emitted per 100 disintegrations of ^{99m}Tc and 98 represents the number of 122 and 136 keV photons emitted per 100 disintegrations of ^{57}Co. For each blood sample, the average of the 2 readings was corrected for radioactivity decay so that the counts represented the activity at the time the sample was collected. The counts

per min per ml at the time of sampling were multiplied by the blood volume of standard man[5200 ml] (66). This product was then related to the counts per minute per microcurie of the equivalent ^{57}Co standard in order to obtain the number of microcuries of ^{99m}Tc present. Thus, knowing the amount of activity injected, the % injected activity was determined and used to find the cumulated activity as described below.

Organ Boundary Definitions

Liver

The shape of the liver is variable. The plasticity of the liver tissue, its regenerative ability, and the pressure exerted by neighboring organs allow a wide variety of configurations. Although the shape of the liver may vary among individuals, or vary over a long period of time within the same individual, it was found that for a patient at rest in a supine position the liver shape remained fairly constant over a 12 hour period [Figure 6].

In order to obtain the liver outline for each scan, the raw data from each detector were processed using the software mentioned in the previous chapter. The image processing options that were used to obtain images similar to those in Figures 4 and 7 are listed below and explained in detail elsewhere (61, 62):

[1] Smoothing with a gaussian matrix, medium wide, weight = 1.

[2] A coarse anti-scatter and anti-penetration correction using a separate table for the upper detector and another for the lower detector. The tables were developed for ^{99m}Tc per instructions (61).

[3] Subtracting n counts from each element where n was dependent upon the amount of background one wished to eliminate.

[4] Division or multiplication of the counts in each element to enhance the image.

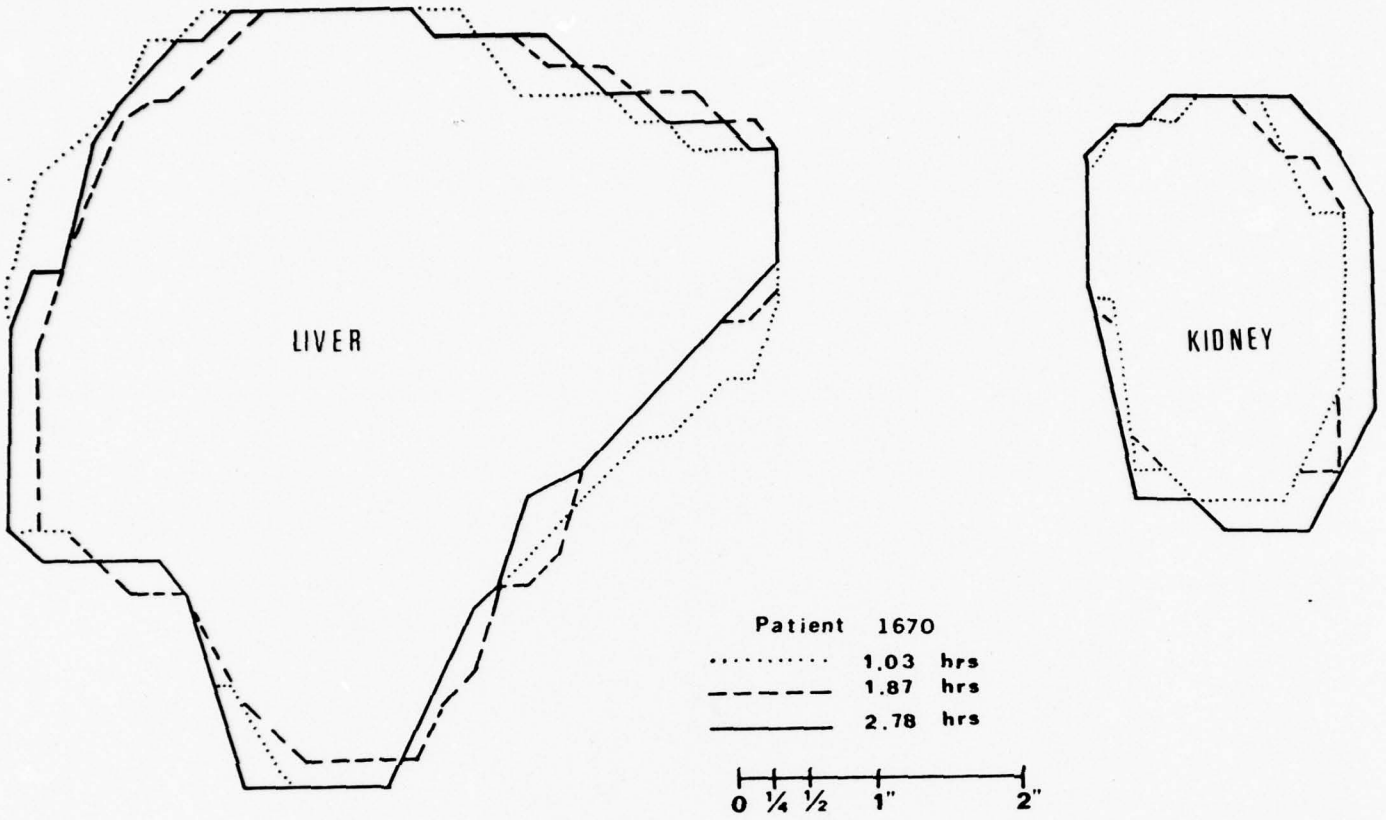

FIGURE 6.

Similarities in organ shapes from different scans.

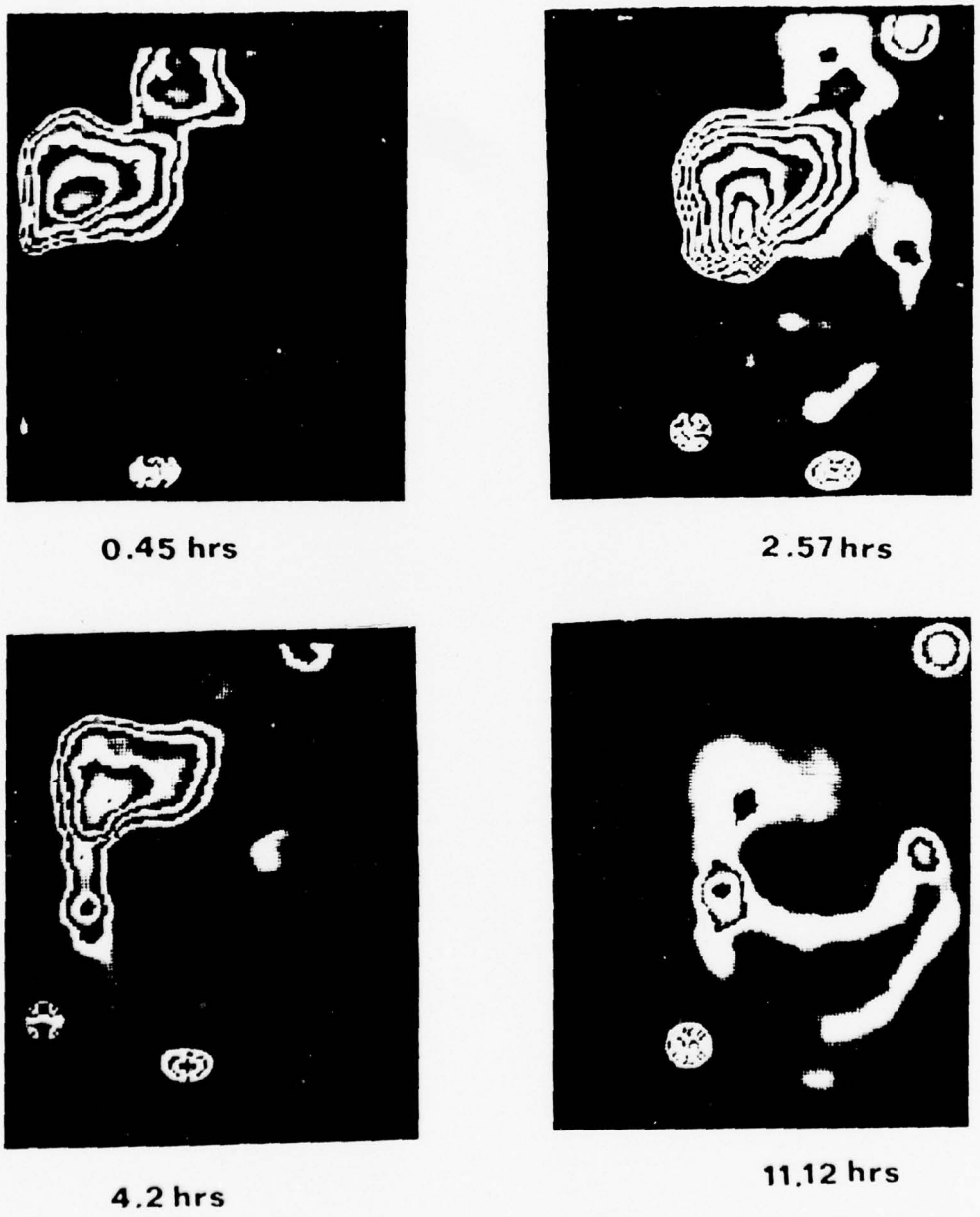

FIGURE 7.

Hepatobiliary clearance of ^{99m}Tc-DHTA

In Figure 7, the heart, liver, and bladder [top to bottom of the image, respectively] can be seen in the 0.45 hours image. At 2.57 hours post-injection, a decrease in the ^{99m}Tc activity in the heart is noted as well as the entry of activity into the intestine. The two circular areas located in the top right and bottom left corners of the image are ^{57}Co spot markers which were used on some patients. By 4.2 hours, noticeable ^{99m}Tc activity in the heart with respect to the liver has almost disappeared and most of the intestinal activity is in the ascending colon. At 11.2 hours, the activity in the liver has decreased significantly and there is now activity in the transverse and descending colon. A reference to Figure 1 may be beneficial to the reader.

It was decided that any further treatment of the data did not significantly aid in organ boundary determinations. With sufficient background subtraction, the non-source organ areas were denoted by zeros on a line printer output of the processed image thereby allowing a simple preliminary outline of the organ boundary. By observing the display and subtracting less counts from each element, an optimal border was established and printed out by the line printer. This output was then superimposed over the preliminary output and another border established using the first as a guide. The outline thus obtained was generally larger than the first since the far edges of the organ were now included whereas in the preliminary determination they may have been subtracted. The resulting border locations thus established were subsequently transferred to the line printer output of the raw data with a variation of perhaps one data element if the count differences so warranted. The above process was performed for both anterior and posterior images.

The established boundaries for the anterior and posterior images were overlaid upon each other and a common liver border was determined using the outermost edge as the common margin. The common liver borders thus established for each scan of a subject were then superimposed and an overall liver boundary was defined using the approximate average of the outlines. As previously noted and seen in Figure 6, the common borders obtained from each scan did not vary significantly for an individual from scan to scan.

The advantage of establishing this overall boundary for each subject and using it as a liver template is evident in those cases where it was difficult to obtain the complete liver outline. In some early and later scans, the separations between heart and liver and between liver and the hepatic flexure of the large intestine were indistinct. When the border separation was unclear, boundary definition in that area was temporarily ignored until overall liver boundary was established for that subject. Then, the liver template was used to approximate the liver outline and to estimate the liver boundary for each scan and each view, employing the right lateral and superior liver margins for orientation.

Background activity was estimated from the average counts per element in the thigh region of each image and multiplying this number by the number of elements within each source organ. This was done separately for anterior and posterior images. The raw counts from each detector within the overall liver boundary were summed and background was subtracted. For the anterior and posterior views of each scan the net counts in the left kidney [determined as described below] were then subtracted to compensate for the contribution of the right kidney to the

observed liver activity. The resulting net counts from the liver recorded by each detector were then used to calculate the geometric mean. Thus, for each image the following applied:

Net Liver Counts = [counts within liver boundary]-[background]-[net kidney counts]

where

background = [# data elemnts within liver boundary] x [average count per element in thigh region]

then,

Liver Geometric Mean = [net liver counts from anterior image x net liver counts from posterior image]$^{1/2}$

Kidneys

For each scan, the border of the left kidney was determined in a manner similar to that described above for the liver except that the processed data from only the lower probe were used for definition of the kdiney margins. The kidney template for each subject was obtained by superimposing the left kidney outlines from each posterior image and then determining an overall kidney boundary. As illustrated in Figure 6, for each subject the shape ofthe kidney did not vary over the period of this study. Then, for each image,

Net kidney counts = [counts within kidney boundary] - [background]

where

background = [# data elements within kidney boundary] x [average count per element in thigh region]

In some scans, radiopharmaceutical in the colon overlapped that in the left kidney making its border obscure, in which case the kidney boundaries were determined using the overall kidney template as described

above for the liver. In such scans, the anterior image was used to outline the colon as illustrated in Figure 7. The average number of net counts per element in the colon where no overlap occurred was determined for each view. Those elements in the kidney region where this count plus background was exceeded were considered to contain both kidney and colon activity. The number of such elements in the kidney region was determined, multiplied by the average count per element in the colon to yield the colon contribution to the kidney counts, and subtracted from the total counts within the kidney region. The remaining counts, which were now considered to be from the kidney alone, were corrected for background activity, as described above for the liver, and the geometric mean of upper and lower detector counts determined for each scan. Therefore,

Net kidney counts = [counts within kidney boundary] - [colon contribution] - [background]

where

colon contribution = [average net count per element in colon where no overlap occurred] x [# of elements within the kidney boundary where the net count per colon element + background was exceeded]

The number of elements involving both kidney and colon were determined for the anterior image and an equal number of elements were assumed to be involved in the posterior image.

The right and left kidneys were considered to be equal in function (67), and thus for dosimetry purposes the total number of counts retained by the kidneys was double that from the left kidney.

Overlap of Left Kidney and Liver

With a few patients, overlap of the left kidney and liver occurred. This situation presented unique complications because now contribution of the liver to kidney counts and vice versa had to be determined. The method utilized in these situations is outlined below.

[1] The organ boundaries were determined as described above. Even when the liver overlapped the left kidney, it was possible to obtain a kidney outline from the posterior image.

[2] The liver and left kidney boundaries were outlined on the same line printer output and the number of common elements determined.

[3] The net counts within the common liver/kidney border were summed.

[4] The data elements in the kidney where no overlap occurred were summed, corrected for background, and averaged to yield the net counts per element in the kidney [Kid_{ce}].

[5] The data elements in the portion of the liver which surrounded the kidney but did not overlap it were summed, corrected for background, and averaged to yield the net counts per element in the liver [Liv_{ce}].

[6] The number of net counts per element in both the kidney [Kid_{ce}] and liver [Liv_{ce}] were then each multiplied by the number of common elements.

[7] The % contribution of the kidney to the sum of the products obtained in step 6 was then determined.

[8] The % kidney contribution was multiplied by the number of net counts in the common elements to obtain the number of counts due to activity in the kidney.

[9] The total net kidney counts are equal to the product obtained in step 8 plus the total net counts in the non-overlap areas of the kidney.

[10] The total net liver counts equal the total net counts within the liver minus the product obtained in step 8 minus the total net kidney counts which were obtained in step 9.

Thus the counts within the liver boundary have been corrected for background, right kidney contribution, and the contribution of the left kidney in the area of overlap.

Intestinal Area

It was possible to define the large intestine Figure 7, but not the time of entry of the activity into each particular segment because of an insufficient number of scans, resulting from the limitations placed by the clinical schedule. The exact division of the large intestine into segments was difficult and the tortuous path of the small intestine limited any detailed definition of that region. Snyder et al. (68) made no attempt to mathematically reconstruct the small intestine and simply considered it as a volume element in their determination of absorbed fractions [Figure 8]. Thus, the small intestine, upper large intestine, and lower large intestine were combined into one intestinal area using the ascending colon as the right margin, the descending colon as the left margin, the caudal margins of the liver and left kidney as the superior intestinal area margin, and the lower portion of the bladder as the inferior margin. The approach to developing an overall intestinal boundary was the same as that used for the liver and kidney.

Determination of Cumulated Activity and Absorbed Dose

Cumulated activity and absorbed dose estimates were obtained utilizing a modified version of a newly developed computer program, MIRD#S, described in detail elsewhere (69, 70). The program was modified to include blood as a source organ utilizing the S-factors for total body.

The cumulated activity in an organ is usually determined by one of two methods. The first method involves the establishment of an exponential expression which describes the radioactivity retention for that organ and then integrating the equation (71-74). The second method entails graphic integration of the activity retention data points (72-73).

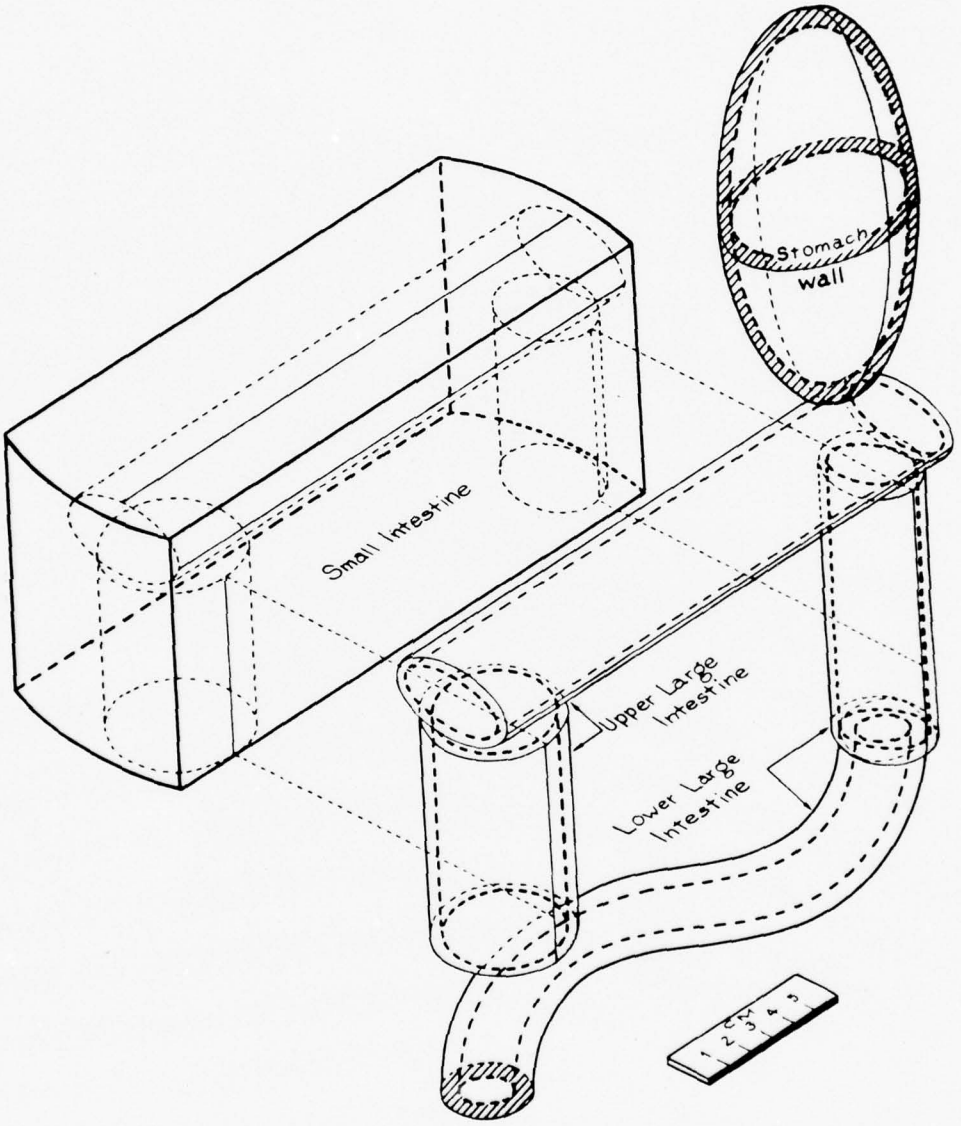

FIGURE 8.

Mathematical model for the gastrointestinal tract*.

*(68)

The latter method was chosen for incorporation into the computer program, MIRD#S. This approach is more practical when a limited amount of data is available, and even if data points are plentiful, reducing the time interval over which the data points are averaged will approximate an exponential if the time interval is small. Physical decay only of the radionuclide was assumed after the last datum point. Absorbed dose estimates were calculated utilizing S-factors (75) and the additivity-of-S principle (76). The recently published S-factors represent a consolidation of physical and anatomic data and may be represented by the following equation:

$$S(r_k \leftarrow r_h) = \Sigma_i \Delta_i \Phi_i (r_k \leftarrow r_h) \qquad \text{rad}/\mu\text{Ci-hr} \qquad (1)$$

where

S = absorbed dose per unit cumulated activity (rad/μCi-hr)

r_h = source organ or volume

r_k = target organ or volume

Δ_i = equilibrium dose constant for particles of i type and energy E_i (gm-rad/μCi-hr)

Φ_i = specific absorbed fraction of energy for target organ r_k for particles i emitted in source organ r_h

It is assumed that the activity is uniformly distributed in the source organ. The phantoms used in estimating specific absorbed fractions are those developed by Snyder et al. (68,75).

The average dose from a specific radionuclide is then determined by:

$$\bar{D}(r_k \leftarrow r_h) = \tilde{A}_h \, S(r_k \leftarrow r_h) \qquad \text{rads} \qquad (2)$$

where

$\tilde{A}_h$ = cumulated activity in source organ r_h

Because several source organs are usually involved, the total mean absorbed dose to a target organ r_k is

$$\bar{D}(r_k) = \Sigma_h \bar{D}(r_k \leftarrow r_h) \quad (3)$$

$$= \Sigma_h \tilde{A}_h S(r_k \leftarrow r_h) \quad (4)$$

In this study, the target organs are the liver [LIV], kidneys, [KID], intestines [IA], ovaries [OV], testes [TST], and red marrow [RM], while the source organs are the liver, kidneys, intestines, and blood. Thus, for example, the total mean absorbed dose to the intestines is represented by

$$\bar{D}_{IA} = \bar{D}_{IA \leftarrow LIV} + \bar{D}_{IA \leftarrow KID} + \bar{D}_{IA \leftarrow IA} + \bar{D}_{IA \leftarrow BLOOD} \quad (5)$$

and

$$\bar{D}_{IA} = \tilde{A}_{LIV} S_{IA \leftarrow LIV} + \tilde{A}_{KID} S_{IA \leftarrow KID} + \tilde{A}_{IA} S_{IA \leftarrow IA} + \tilde{A}_{BLOOD} S_{IA \leftarrow BLOOD} \quad (6)$$

The above example actually represents the most complex dose determination in this study since S-factors are not tabulated for the blood and total intestinal area. Since blood can be considered as uniformly distributed throughout the body, the S-factors for total body were used for the blood. S-factors are tabulated for the small intestines, upper large intestines, and lower large intestines and by using the additivity of S concept (76) an S-factor for the total intestinal area was established.

The additivity of S concept assumes that

$\{ X_i \}_{i=1}^{n}$ $\{ Y_j \}_{j=1}^{m}$

are any sets of discrete organs or regions of the body represented

collectively by V and W, respectively. If the activity is uniformly distributed within the source volume W, the fraction of the total energy emitted by source region Y_j is M_{Y_j} / M_W where M_{Y_j} is the mass of source region Y_j and M_W the total mass of the source regions within W, and the energy is additive among regions. Thus

$$S\ (V \leftarrow W) = \Sigma_j S(V \leftarrow Y_j) \frac{M_{Y_j}}{M_W} \tag{7}$$

Similarly, the fraction of energy absorbed by the target organ X_i is M_{X_i} / M_V and

$$S\ (V \leftarrow W) = \Sigma_i S(X_i \leftarrow W) \frac{M_{X_i}}{M_V} \tag{8}$$

Therefore,

$$S\ (V \leftarrow W) = \Sigma_i \Sigma_j S\ (X_i \leftarrow Y_j) \frac{M_{X_i} M_{Y_j}}{M_V M_W} \tag{9}$$

By applying this concept to the intestines [IA] which are comprised of the small intestines [SI], the upper large intestines [ULI] and the lower large intestines [LLI], the total mean absorbed dose to the intestines [equation 6] is expressed by the following:

$$\begin{aligned}
\overline{D}_{IA} = {} & \tilde{A}_{LIV}\left[S_{SI \leftarrow LIV} \frac{M_{SI}}{M_{IAW}} + S_{ULIW \leftarrow LIV} \frac{M_{ULIW}}{M_{IAW}} + S_{LLIW \leftarrow LIV} \frac{M_{LLIW}}{M_{IAW}}\right] \\
& + \tilde{A}_{KID}\left[S_{SI \leftarrow KID} \frac{M_{SI}}{M_{IAW}} + S_{ULIW \leftarrow KID} \frac{M_{ULIW}}{M_{IAW}} + S_{LLIW \leftarrow KID} \frac{M_{LLIW}}{M_{IAW}}\right] \\
& + \tilde{A}_{IA}\left[\left(S_{SI \leftarrow SI} \frac{M_{SI} M_{SI}}{M_{IAW} M_{IAC}} + S_{SI \leftarrow ULIC} \frac{M_{SI} M_{ULIC}}{M_{IAW} M_{IAC}}\right.\right. \\
& \left. + S_{SI \leftarrow LLIC} \frac{M_{SI} M_{LLIC}}{M_{IAW} M_{IAC}}\right) + \left(S_{ULIW \leftarrow SI} \frac{M_{ULIW} M_{SI}}{M_{IAW} M_{IAC}}\right. \\
& \left.\left. + S_{ULIW \leftarrow ULIC} \frac{M_{ULIW} M_{ULIC}}{M_{IAW} M_{IAC}} + S_{ULIW \leftarrow LLIC} \frac{M_{ULIW} M_{LLIC}}{M_{IAW} M_{IAC}}\right)\right]
\end{aligned}$$

$$+ \left(S_{LLIW \leftarrow SI} \frac{M_{ULIW} M_{SI}}{M_{IAW} M_{IAC}} + S_{LLIW \leftarrow ULIC} \frac{M_{LLIW} M_{ULIC}}{M_{IAW} M_{IAC}}\right.$$

$$\left. + S_{LLIW \leftarrow LLIC} \frac{M_{LLIW} M_{LLIC}}{M_{IAW} M_{IAC}} \right)] + \tilde{A}_{BLOOD} [S_{SI \leftarrow BLOOD} \frac{M_{SI}}{M_{IAW}}$$

$$+ S_{ULIW \leftarrow BLOOD} \frac{M_{ULIW}}{M_{IAW}} + S_{LLIW \leftarrow BLOOD} \frac{M_{LLIW}}{M_{IAW}}] \qquad (10)$$

where W = wall

C = contents

The equation for the total mean absorbed dose to the other target organs is simplier as seen in the following example for the liver.

$$\bar{D}_{LIV} = \bar{D}_{LIV \leftarrow LIV} + \bar{D}_{LIV \leftarrow KID} + \bar{D}_{LIV \leftarrow IA} + \bar{D}_{LIV \leftarrow BLOOD}$$

$$= \tilde{A}_{LIV} S_{LIV \leftarrow LIV} + \tilde{A}_{KID} S_{LIV \leftarrow KID} + \tilde{A}_{IA} [S_{LIV \leftarrow SI} \frac{M_{SI}}{M_{IAC}}$$

$$+ S_{LIV \leftarrow ULIC} \frac{M_{ULIC}}{M_{IAC}} + S_{LIV \leftarrow LLIC} \frac{M_{LLIC}}{M_{IAC}}]$$

$$+ \tilde{A}_{BLOOD} S_{LIV \leftarrow BLOOD}$$

The biological retention of ^{99m}Tc-DHTA by the source organs is observed if the data are corrected for radioactive decay. Such data analysis gives an indication of the biological treatment of the pharmaceutical by a particular organ assuming that the bond with the radioactive tracer has not been broken. An option of the computer program, MIRD#S, which provides a listing of the % injected activity corrected for radionuclide physical decay plus a plot of the results (69,70) was

utilized to study the biological movement of the radiopharmaceutical.

CHAPTER VI

RESULTS

General

Cumulated activity and absorbed dose determinations were made for each individual. In addition, the data from all patients were averaged over 0.5 hour intervals, and cumulated activity and absorbed dose values were determined for the combined data set [Appendix 4].

Since sufficient blood samples from any one individual were not available for an accurate analysis, only the combined data set averaged over 0.1 hour time intervals was used to determine the cumulated activity in blood. This cumulated activity value was then used in all absorbed dose calculations.

Biological Retention of ^{99m}Tc-DHTA

Figure 9 shows a typical biological retention curve for ^{99m}Tc-DHTA in the liver. The buildup of the pharmaceutical in the liver which occurs during the first 3 hours corresponds to the removal of DHTA from the blood by the hepatocytes, its secretion into the biliary system, and its retention by the gall bladder. The concentration of DHTA begins to reduce shortly after 3 hours which corresponds to the first fatty meal and the emptying of the gall bladder into the duodenum. A gradual but continuous decrease is then evident with about 13% of the pharmaceutical remaining after 12 hours.

In Figure 10, the biological treatment of DHTA by the kidneys can be observed for a typical subject. There is a gradual increase in concentration from approximately 5 to 6% of the administered dosage from 1 to

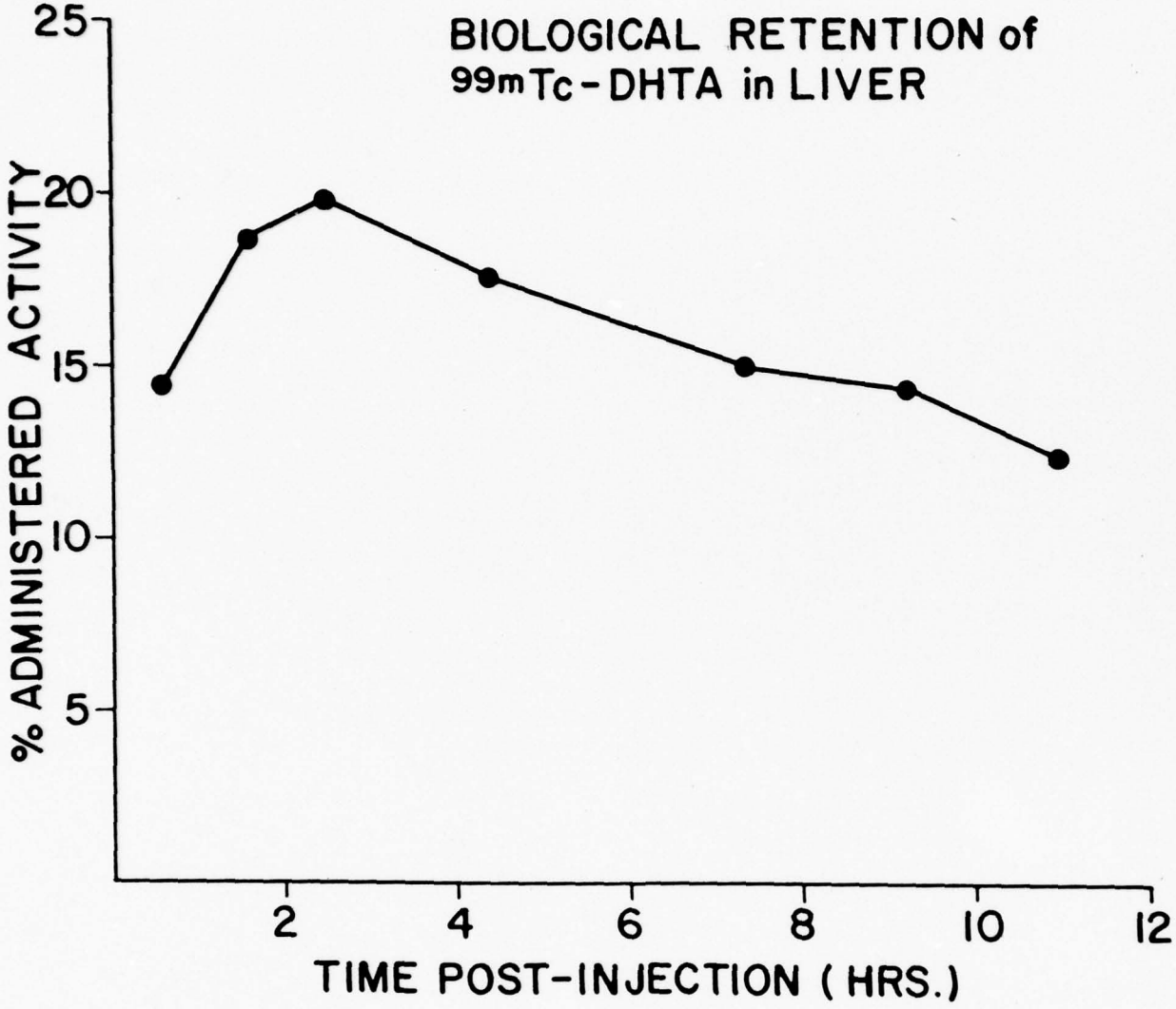

FIGURE 9.

Biological retention of ^{99m}Tc-DHTA in liver.

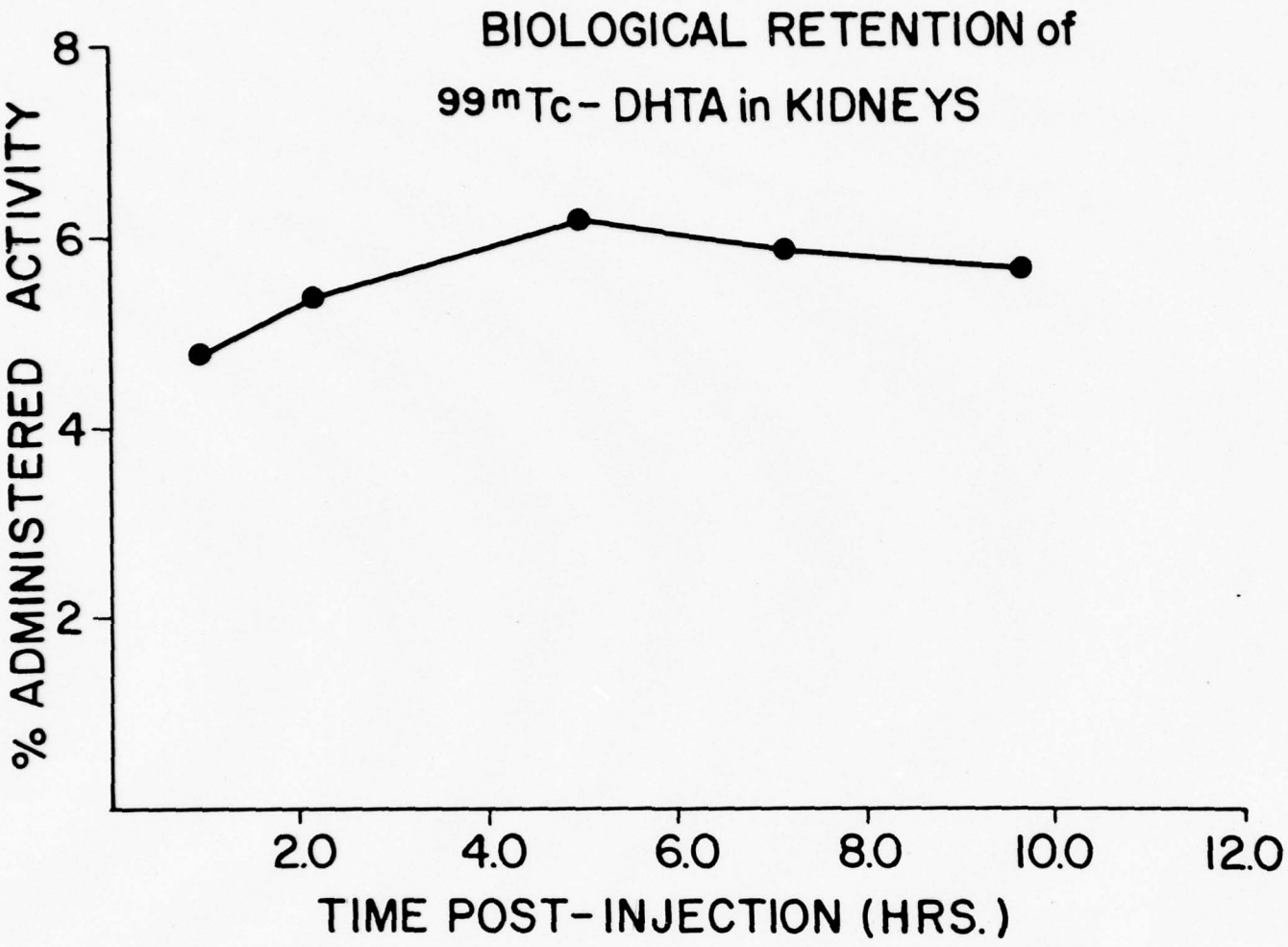

FIGURE 10.

Biological retention of ^{99m}Tc-DHTA in kidneys

5 hours respectively after which a very slight decrease occurs. At 10 hours post-injection, about 5% of the pharmaceutical remains in the kidneys.

Intestinal motility varies greatly among individuals and even within the same individual at different times. The degree of motility is the prominent factor affecting the retention of DHTA by the intestines. Figure 11 serves only to illustrate that for a typical subject there is a continuous buildup of DHTA in the intestines due to the continual influx of bile until some point at which the individual defecates.

Figure 12 is a composite curve of data from 9 patients, as described earlier, illustrating the retention of DHTA in the blood. During the first hour there is a very steep reduction in the DHTA concentration from almost 92% at 0.2 hours to 40% at 1.0 hour. The decrease continues at a fairly rapid rate during the next two hours to about 25% at 3.0 hours. Thereafter, the decrease is more gradual, declining to 10% at 11 hours post-injection.

Activity Retention of ^{99m}Tc-DHTA

The absorbed dose to the various target organs depends upon the amount of radioactivity retained by the body. Thus both the biological clearance of the pharmaceutical and the physical decay of the radionuclide have an effect upon the absorbed radiation dose.

Representative activity retention curves of some typical source organs are shown in Figure 13-16. The activity retention curve of the liver [Figure 13] is similar to its biological retention curve [Figure 9] except that the rate of uptake is slower and the rate of clearance is more rapid due to the inclusion of radioactive decay. The activity reaches a maximum of 15% at 2.0 hours and then decreases to 3% at 12 hours. The activity in the kidney [Figure 14] is 4% of the administered dosage

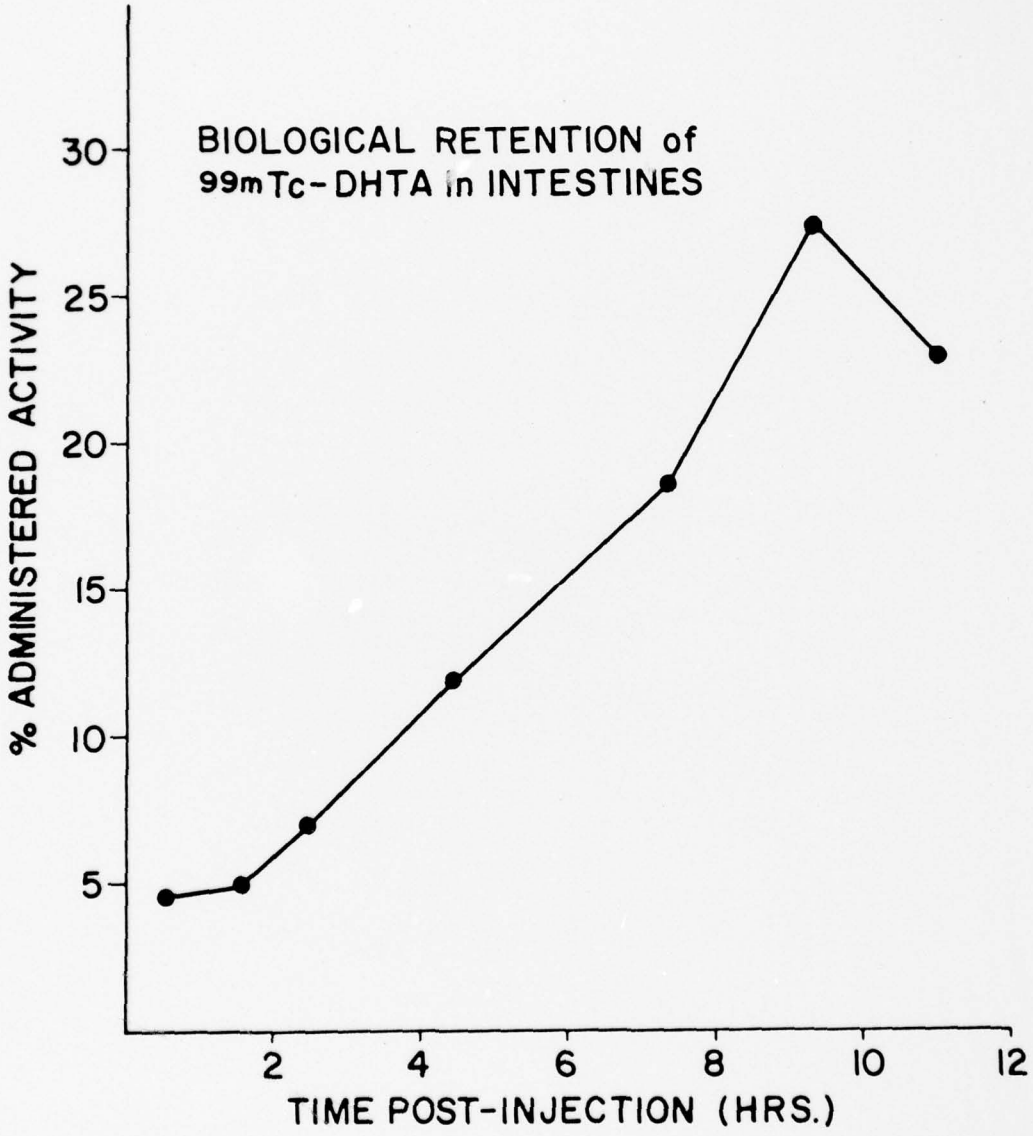

FIGURE 11.

Biological retention of ^{99m}Tc-DHTA in intestines.

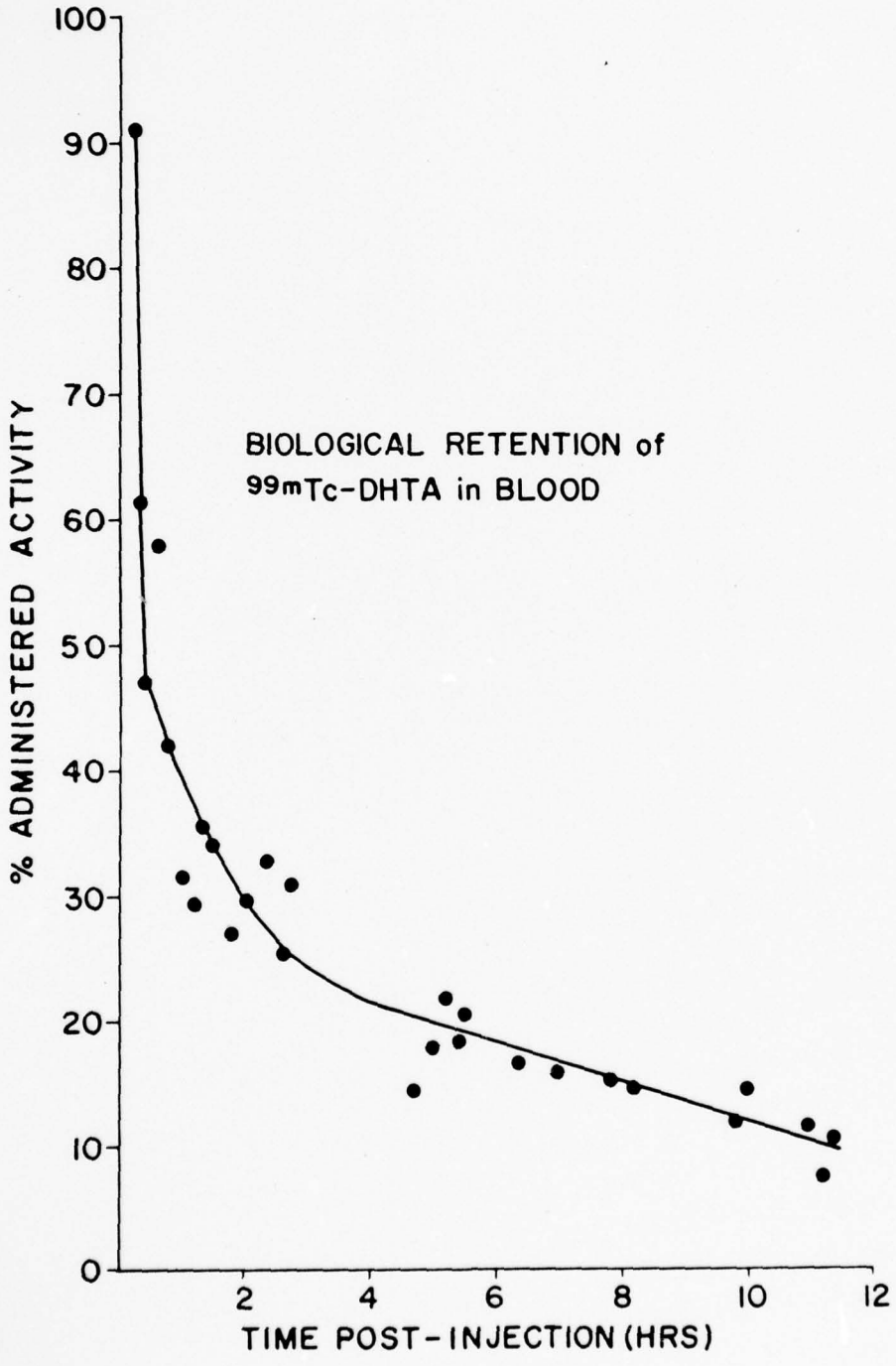

FIGURE 12.

Biological retention of ^{99m}Tc-DHTA in blood.

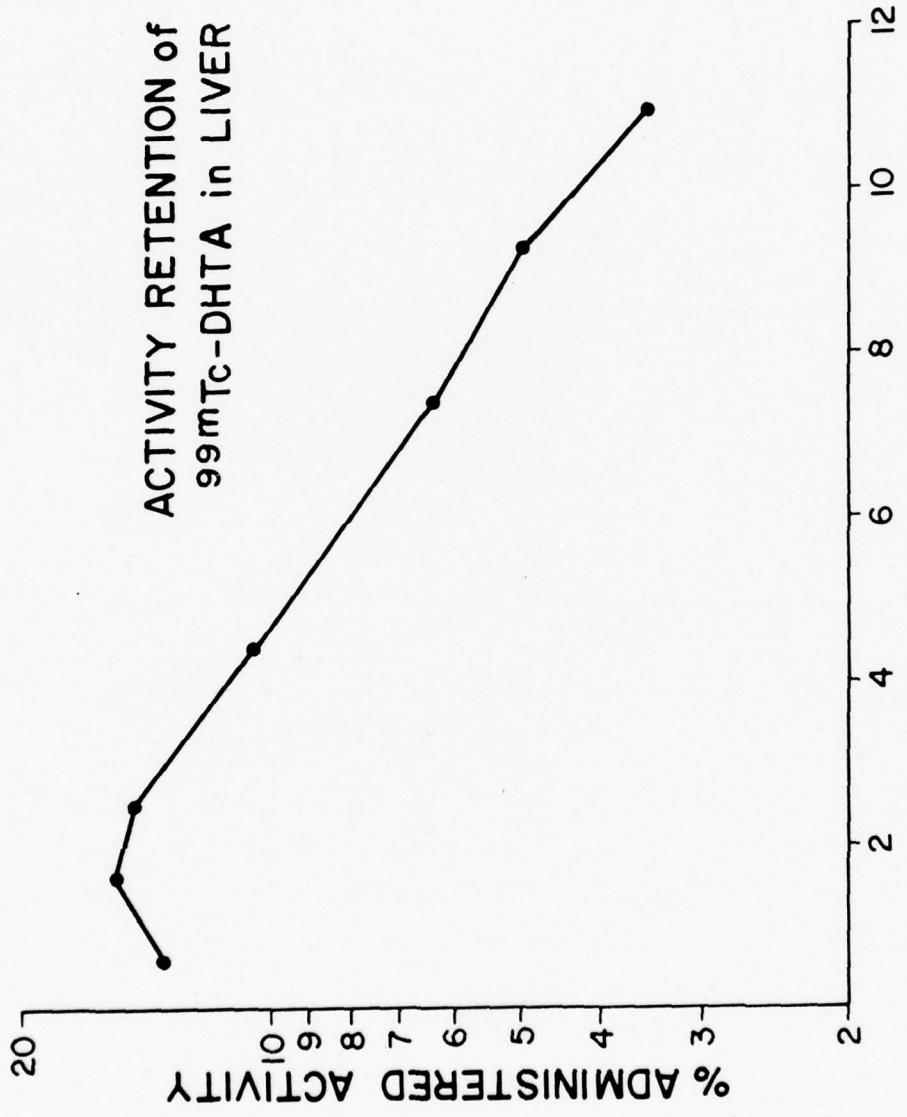

FIGURE 13.

Activity retention of ^{99m}Tc-DHTA in liver.

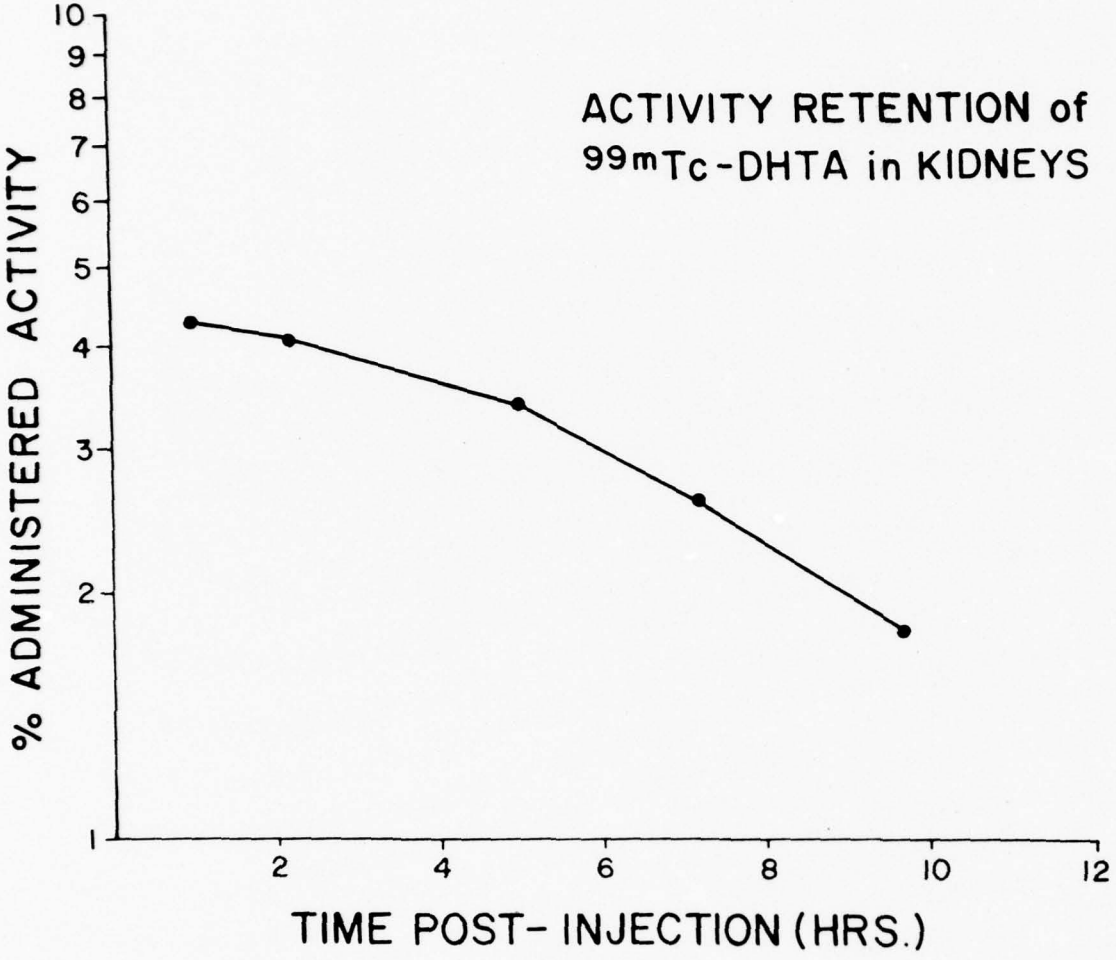

FIGURE 14.

Activity retention of ^{99m}Tc-DHTA in kidneys.

shortly after injection and declines to less than 1% after 12 hours. The representative curve for the intestines [Figure 15] shows an increase in activity to almost 10% before the patient defecated. The composite blood curve [Figure 16] shows the rapid decrease during the first hour from almost 90% to around 35%, decreasing more gradually to 18% at 3.0 hours and then to less than 3% at 12 hours.

Cumulated Activity and Absorbed Dose Estimates

Cumulated activity and absorbed dose were determined for each of the 19 individuals as well as a combined data study. Values for blood, however, were based only on the combined data. The values obtained are presented in Appendix 4 and summarized in Tables 8 and 9.

TABLE 8

CUMULATED ACTIVITY (μCi-hrs/mCi administered)

Source	Individual Range	Individual Mean (of 19)	s.d.
Liver	825-2250	1273	246
Kidneys	108-810	352	167
Intestines	391-1310	822	257
Blood	N/A	2002	N/A

The emphasis and final internal radiation absorbed dose estimates given in this study are based on the geometric mean of the counts from the upper and lower detectors. However, absorbed dose estimates were also determined using the arithmetic mean [Appendix 5] and a comparison made between the two sets of results [Appendix 6].

FIGURE 15.

Activity retention of ^{99m}Tc-DHTA in intestines.

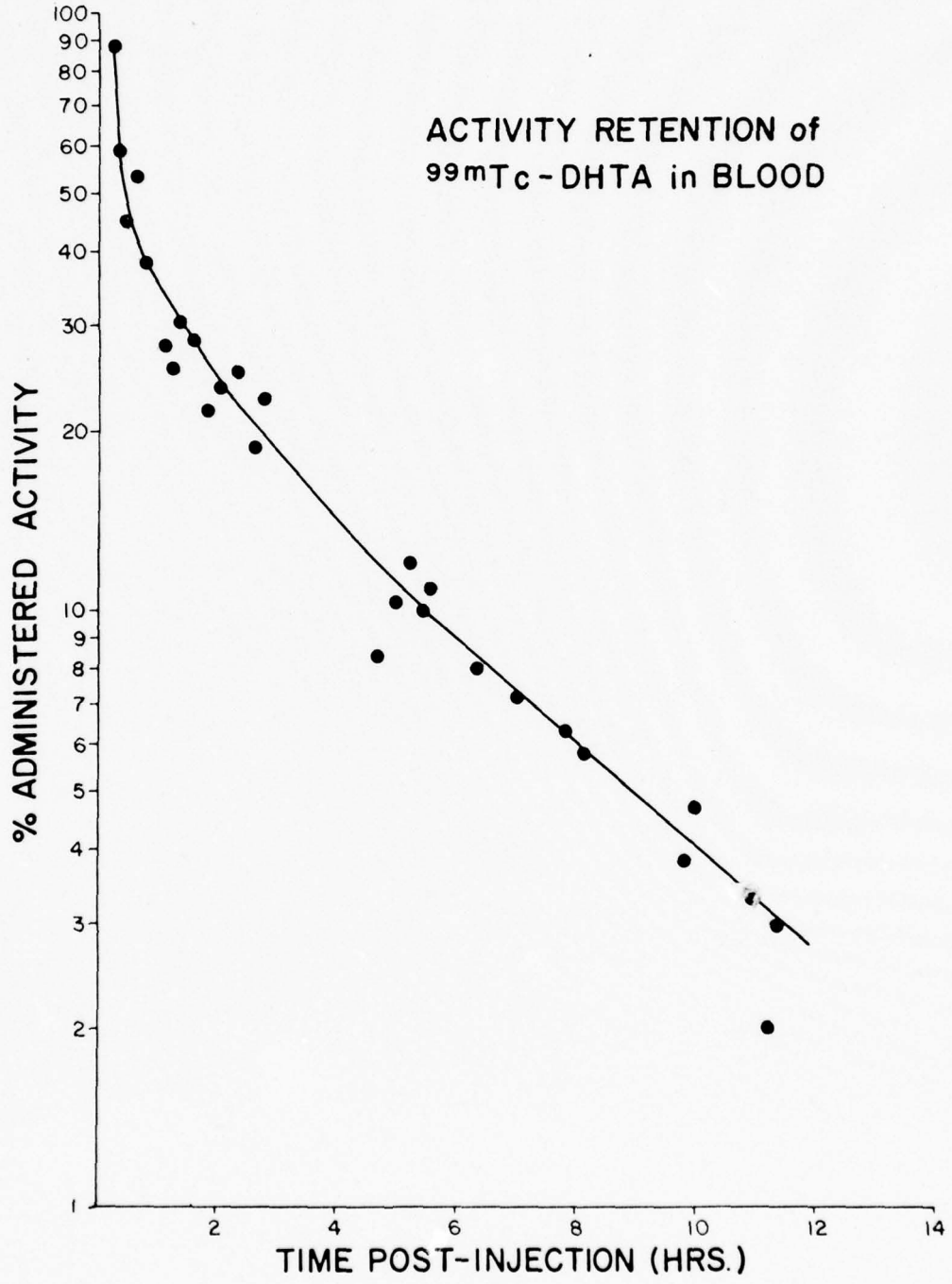

FIGURE 16.

Activity retention of ^{99m}Tc-DHTA in blood.

TABLE 9

ABSORBED DOSE (mrads/mCi administered)

Target Organ	Individual Range	Individual Mean (of 19)	s.d.
Liver	46-110	66	17
Kidneys	31-164	79	32
Intestines	29-79	53	14
Ovaries	10-21	15	3
Testes	3-4	3.8	0.1
Red Marrow	10-16	13	2

CHAPTER VII

DISCUSSION AND CONCLUSIONS

Data Acquisition Techniques

Several methods have been utilized by researchers in their attempts to obtain quantitative human data *in vivo*. Radiation detection probes have been placed over organs to record changes in count rates and have also been coupled to flat field collimators to obtain the counts within the organ. Changes in the count rate from a particular region may give an indication of radioactivity turnover within the organ but do not give a good estimate of the amount of activity in the entire organ due to variations in organ size and inaccuracies of probe positioning. The use of flat field collimators does not allow for consideration of activity contributions from surrounding tissues. Thus all activity within the collimator's field of view was considered as being within the organ. The laborious technique of counting dots on a scan has been utilized in some studies (56, 77, 78) but has understandably never achieved popularity.

Quantitative profile scanning has also been investigated (59, 78). This technique usually involves specialized equipment and has problems in the assignment of peaks to particular organs, the separation of peaks from adjacent concentrations, and the establishment of a baseline corresponding to the general "background" activity. Frequently, limited human data (e.g., blood, excreta, whole body retention measurements) have been combined with organ data from animals in order to obtain

absorbed dose estimates. Animal data, however, can seldom be directly related to humans with any significant degree of reliability.

Computers interfaced with scanners and gamma cameras have been utilized for quantitative data acquisition and analysis. In one case utilizing the computer (79), unwanted regions were shielded from detection thereby facilitating data collection and analysis. In another study where this approach was not feasible (80), photoscans were used to aid in organ definition and the total counts within a rectangular area which enclosed the organ of interest were obtained. Although organ boundary definition was somewhat subjective and the use of rectangular regions to enclose irregularly shaped organs introduced some error, this approach did show significant progress in obtaining quantitative human data in vivo. One other recent study (81), utilized a gamma camera with a diverging collimator to image portions of two separate organs and the activity changes within those regions were studied. These data plus animal data were used for absorbed dose determinations. Besides the problems of recording count rate changes in only portions of organs and using animal data, the diverging collimator increases field size with depth. Obviously, no approach has yet proved to be the panacea and each has its own imperfections.

The method used in this investigation to obtain quantitative human data in vivo required first identifying the organ boundaries by correcting for scatter within the body [antiscatter corrections], smoothing by a matrix averaging process, and subtracting background. Although the above data processing options were invaluable in organ boundary definition, their affect upon the observed counts for dosimetry purposes was unknown and thus the "raw" counts minus corrections for background and organ

overlap were used to determine the activity within the organ. This technique introduces new concepts and methods for organ boundary definition and compensation for overlapping organs which eliminate the subjectivity encountered in the past.

Intestinal Tract Dosimetry

Regarding estimates of the absorbed dose to the intestinal tract Bernard and Hayes noted, "A rigorous model would take into account the following factors: [1] geometry of the tract, [2] concentration and rate of movement of activity down the tract, [3] nuclide absorption from the tract, [4] secretion of nuclide into the tract..., [5] dilution of the lumen content by secretion of digestive fluids, [6] concentration of the tracer by absorption of water and nutrients from the tract, [7] irradiation from other organs or adjacent tract, [8] radioactive decay of parent and buildup of daughters, and [9] type and energy of radiations involved" (82). Add to these the absorption of radiation by the intestinal contents and mucosal lining plus the variation in the rate of movement through the intestines among individuals and even in the same individual and the model becomes extremely complex.

Several theoretical models (82, 83) have been proposed for estimating the absorbed dose to the intestines. These models, however, still require data such as the initial activity [or rate of activity] entering the gastrointestinal [GI] tract. It should also be emphasized that these models are theoretical and their accuracy could be enhanced with supplementary *in vivo* data.

The geometric complexity of the GI tract has been simplified by Snyder and associates (68) who have given mathematical descriptions of body organs used to estimate absorbed fractions. The small intestine

was considered as a section of a circular cylinder excluding the portion occupied by the large intestine which was represented by cylinders, elliptical cylinders and an S-shaped figure [Figure 8]. No allowance was made for the cephalic upswing of the transverse colon to the splenic flexure [Figure 1]. Even with the aid of these theoretical models and geometric equations, it was still necessary for the MIRD committee (84) to estimate the temporal distributions of ^{131}I-labeled sodium rose bengal in the biliary tract, gall bladder, and small intestines from clinical records of sequential scintophotos because the necessary quantitative data were lacking.

The approach taken for the intestinal area in this study was by necessity rather basic; however, it represents the first quantitative in vivo determination of intestinal activity using external area scanning. Besides the anatomical complexity of the intestinal area which obscured adequate and consistent intestinal segment definition, the limited availability of the equipment, the inability of the patients to tolerate frequent scanning, and the variations in intestinal motility made it impossible to determine the exact time of entry of the radionuclide into each segment. Thus any division of the intestines into segments [e.g., small intestines, upper large intestines, and lower large intestine] would be unavailing. Since the S-factors are based on a volume element for the small intestine and the upper large intestine and part of the lower large intestine lie within that element (68, 75) the concept of unifying the segments into one volume is not unreasonable. Derivation of the S-factors assumes also uniform distribution of activity within a segment as do some of the theoretical equations (82) while in reality the activity does not mix instantly within each segment nor does it all leave or enter each segment at a definite time.

Since the subjects in this study had been NPO for almost 12 hours before the first meal after radionuclide injection, the movement of the activity through the small intestine was rapid. Once the activity reached the caecum, however, a more sluggish movement through the ascending colon was noted thus possibly creating a larger absorbed dose to this segment than that calculated for the intestinal area. However, in Figure 7 a bolus-like movement of activity through the ascending colon is noticed followed by a more general mixing through the transverse colon. It appears that much of the activity is eliminated from the body with the defecation containing the primary bolus thereby creating a rapid decrease in activity due to biological elimination. By assuming physical decay only after the last datum point was collected, this major decrease in activity due to biological elimination was generally ignored thus resulting in a higher overall estimated dose. The bolus of activity may create a higher dose at a particular location than one would estimate with a uniform distribution but once the bolus had passed, a lower dose would result. Therefore, assumption of a uniform distribution and physical decay only after the last datum point represents a good compromise. It should be emphasized that the dominant factor in determining the absorbed dose to the intestines is the rate of movement of the activity. Any positive action to accelerate this movement will reduce the absorbed dose.

Biological Treatment of ^{99m}Tc-DHTA

It is interesting to relate the concentration of DHTA in the blood to that in other source organs. The dramatic decrease in the blood during the first 4 hours [Figure 12] corresponds to the time of increase in the liver and kidneys [Figures 9 and 10]. After 4 hours, however, there is a relatively slow decrease in the blood concentration from approximately

20% of the injected concentration to 10% at 11.5 hours. During this same time period, the DHTA concentration in the liver decreases from 18.5% to almost 12% while the kidney concentration remains a relatively constant 5-6% and the intestinal concentration increases.

If one recalls from Chapter III that lipoic acid is thought to be an essential vitamin and is found widely distributed in food as well as synthesized by the intestinal flora, a plausible hypothesis for the biological treatment of ^{99m}Tc-DHTA by the source organs can be developed. First consider that kidneys not only excrete the end-products of bodily metabolism but also reabsorb essential substances thereby controlling the concentration of most body fluid constituents (85, 86). The reabsorption process is either passive or active. Active reabsorption has a limited capacity for various substances, the capacity limit noted as the tubular maximal reabsorption capacity (TM). If the TM is exceeded by a particular substance, that substance will then appear in the urine Conversely, if the TM is not exceeded, the substance will not appear in the urine because it is being totally reabsorbed in the tubules.

If if is assumed that lipoic acid is an essential vitamin which is selectively reabsorbed by the body and that ^{99m}Tc-DHTA behaves *in vivo* as lipoic acid, then the following can be deduced.

After injection of ^{99m}Tc-DHTA into the blood, the liver hepatocytes rapdily remove it from the blood until a saturation point is reached. Then, after secretion of some bile [containing ^{99m}Tc-DHTA] into the intestine, the hepatocytes are able to remove more of the radiopharmaceutical from the blood. This increase in concentration is, however, offset by further bile secretion thus resulting in a net decrease in the concentration of ^{99m}Tc-DHTA in the liver. Meanwhile the kidneys are removing the

radiopharmaceutical from the blood but a portion is being reabsorbed back into the blood stream. Since the TM has been exceeded, there is secretion of ^{99m}Tc-DHTA into the urine which over a period of time is gradually reduced as the TM is approached. Added influx of ^{99m}Tc-DHTA is provided by the intestines. Since lipoic acid is manufactured by the intestinal flora, some enterohepatic [intestine to liver] circulation probably occurs.

The above analysis is indeed a hypothesis which requires a detailed physiological and biochemical analysis. An important ramification of this mode of biological treatment of DHTA by the kidney is that dose estimates based on urine collections would be erroneously low and that this concept can be extended to other radiopharmaceuticals whose biological treatment by the kidneys is uncertain.

Error Considerations

The estimated absorbed radiation doses presented in Table 9 should be applied with their limitations understood. Precise organ boundary definitions are difficult to obtain, especially when one scan requires 15 min during which time the organ location may vary slightly and the radioactive concentration within the organ may change. It is also impossible to create an accurate phantom which would represent a dynamic physiological process and also account for the contribution from surrounding organs. An appropriate background is also difficult to establish, for just the degree of vascularization alone can create variations. Other physiological and anatomic consdierations which apply are the variations in rate of uptake and removal of the radiopharmaceutical due to organ size and functional activity [e.g. a cirrhotic liver will remove ^{99m}Tc-DHTA slower than a normal liver], early or late release of

bile into the intestines, and the normal and abnormal variations in intestinal motility.

Most of the limitations of the S-factors have been defined elsewhere (68, 75, 76) but it must be emphasized that these calculations apply only to a 70 Kgm human with standard organ weights and configurations and a uniform distribution of the radionuclide within each tissue. The dose to the right and left kidneys were assumed equal while in reality they would be different due to different anatomical locations. The use of total body S-factors for blood introduces some error because it ignores any blood pools and assumes a uniform distribution.

With these limitations in mind, the absorbed radiation dose estimates presented in this manuscript may be beneficially applied.

Dose Comparisons With Other Agents

A comparison of the absorbed radiation dose from ^{99m}Tc-DHTA and other selected imaging agents is made in Table 10. The reported values depend heavily upon the techniques utilized to obtain the quantitative data necessary for absorbed dose determinations. Values for other imaging agents can be found in a summarized form elsewhere (87). The only comparable agents with ^{99m}Tc-DHTA are ^{131}I and ^{123}I rose bengal. ^{198}Au colloid, ^{113m}In colloid, and ^{99m}Tc iron hydroxide and sulfur colloid are RES cell imaging agents, while ^{131}I iodohippurate is used in kidney function studies and ^{99m}Tc MAA is a lung scanning agent. In comparison with these listed agents, ^{99m}Tc-DHTA gives the lowest or one of the lowest doses to the tabulated target organs, and thus compares very favorably to agents routinely used in clinical investigations.

Recommendations

It is difficult to recommend a particular amount of activity to

TABLE 10

ABSORBED DOSE (mrad/uCi) FROM INTERNALLY ADMINISTERED ISOTOPES*

Radio-nuclide	Radio-pharmaceutical	Liver	Kidneys	Intestines	Ovaries	Tests	Red Marrow
^{131}I	rose bengal**	0.8	------	52.5	1.6	0.14	0.32
	iodohippurate	0.06	0.4-1.0	----	---	0.02-0.1	----
^{123}I	rose bengal**	0.19	------	3.5	0.28	0.014	0.08
^{198}Au	colloid	30-40	8	----	----	0.1-0.3	2-7
^{113m}In	colloid	0.1-0.6	-------	----	----	0.02	0.02
^{99m}Tc	iron hydroxide	0.1-0.5	0.5-1	----	----	0.02-0.05	0.02
	sulfur colloid	0.2-0.4	------	----	----	0.01-0.2	0.02-0.03
	MAA	0.07-0.08	0.1-0.2	----	----	0.01-0.02	----
	DHTA***	0.066	0.079	0.053	0.015	0.004	0.013

*(87) unless otherwise noted.
**(84)
***Results of this study.

employ in the clinical situation since the primary objective is to obtain optimum information at the lowest practicable dose. The size and age of the patient as well as his clinical condition are all factors which should be taken into consideration before determining the injected activity. In relationship to other imaging agents such as ^{131}I and ^{123}I rose bengal and ^{99m}Tc-sulfur colloid at least twice the amount of ^{99m}Tc-DHTA could be administered if needed without exceeding the absorbed dose from those agents. However, the 4 mCi dosage recommended by the manufacturer seems adequate for producing in the normal adult patient clinically meaningful results. This amount should be used as the basic guideline.

The use of ^{99m}Tc-DHTA to analyze liver function should be investigated. With the advent of computers in nuclear medicine, quantitative dynamic liver function studies could be performed. The rate of removal of ^{99m}Tc-DHTA by the liver during the first 5-10 minutes may be clinically significant. In some clinical studies (2), ^{99m}Tc-DHTA appeared to be more sensitive to liver malfunction than ^{99m}Tc-sulfur colloid. The biological behavior of ^{99m}Tc-DHTA is another area which warrants further study. Does ^{99m}Tc-DHTA behave in vivo as lipoic acid and can it be used as a lipoic acid tracer? Perhaps an investigation into the enterohepatic circulation of ^{99m}Tc-DHTA would prove of value in diagnosing malabsorption of lipoic acid. If lipoic acid is an essential vitamin, this would be clinically meaningful. Finally, a comparison of the absorbed radiation dose obtained by quantitative in vivo determination of kidney activity to that obtained by urine collection would prove beneficial in determining the amount of DHTA absorption by the kidneys and would illustrate the significance of each method in absorbed dose calculations.

APPENDIX 1

THE EFFECT OF VARYING THE DISTANCE FROM THE DETECTOR TO SOURCE

Williams et al. (56) stated that "a detector with a fine focusing collimator which scans over a large area may be considered as a very large fixed detector similar in physical characteristics to a gamma camera with a large crystal and a multi-parallel-hole collimator. With these systems, the variation in sensitivity due to the inverse square law is eliminated unless the source is very close to the detector or is large compared with the effective detector size." Essentially the same observation has been made by others (57-60). For the instrumentation used in this study, the effects of source-to-detector distance were studied in order to ascertain if they were indeed negligible.

A rectangular plexiglass volume phantom, 20 x 13 x 8 cm filled with water and 5.38 mCi of eluate from a ^{99}Mo-^{99m}Tc generator, was scanned with 3.8 cm of pressed wood between the phantom and each detector and the following settings on the rectilinear scanner described in Chapter IV:

[1]	scan speed	500 cm/min
[2]	longitudinal speed	750 cm/min
[3]	centerline	140 keV
[4]	window	±20 keV
[5]	line spacing	0.25 inches

The lower probe was at a constant distance of 1.5 cm from the top of the scanning table and the upper probe at variable distances. This best

represents the study situation since the lower probe was kept at this constant distance for different patients but the position of the upper probe varied to accommodate different patient thicknesses.

The numbers of counts within the rectangular areas of interest from each detector were determined using the PDP 8/I computer [also described in Chapter IV] and then corrected for radioactive decay. The geometric mean for each scanning situation was determined and, as can be seen in Figure A-1, did not vary by more than 3.7% as the distance of the upper probe from the absorber increased by 16 cm. This corresponded to moving the upper detector from 22.5 to 38.5 cm from the table top. In the studies reported in this dissertation, the distance of the upper probe from the table top varied only from 26.0 to 31.0 cm, which corresponds to less than 1% count variation [see Figure A-1].

Thus the 5.0 cm variation in the distance of the upper detector from the table top encountered during patient data collection had a negligible effect upon the detected organ counts.

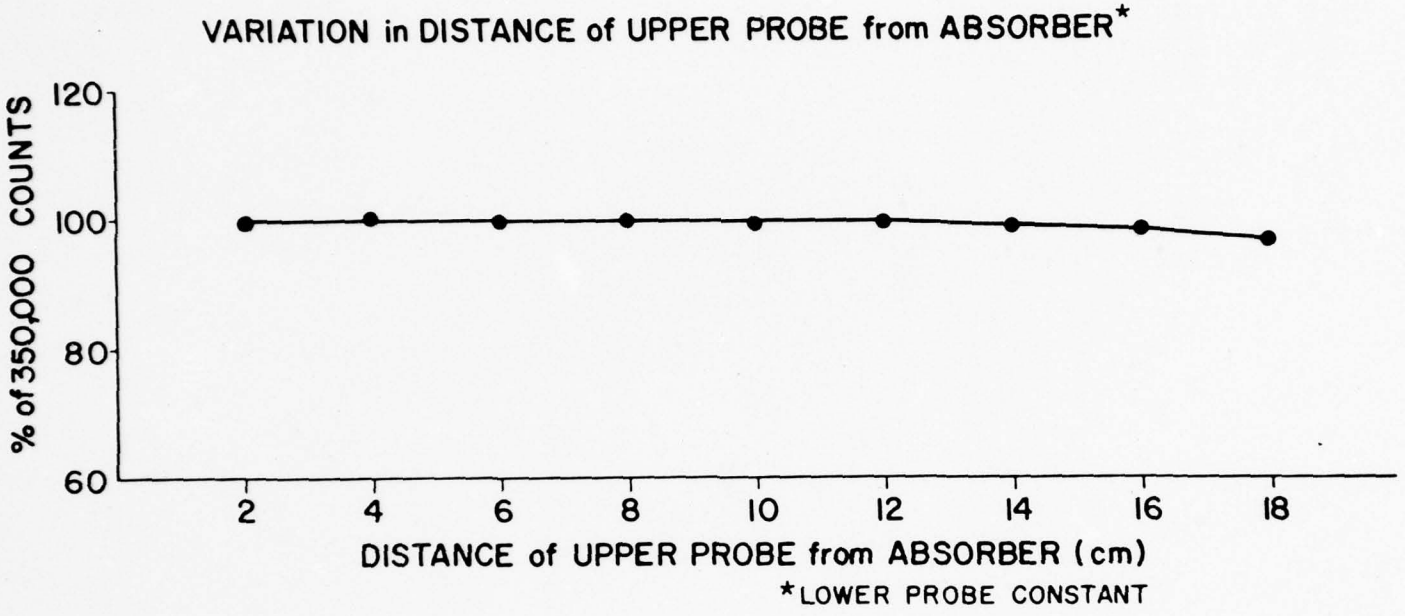

FIGURE A-1

Variation of geometric mean with increasing distance of upper detector from absorber

APPENDIX 2

THE EFFECT OF VARYING THE SOURCE POSITION BETWEEN TWO FIXED DETECTORS

In 1937, Evans (88) first introduced the concept of minimizing the effects of source depth within a body by making two symmetrical measurements, one with the patient's back toward the detector and the second with the patient facing it, and then using the geometric mean of conjugate counts. Hisada et al. (89) in 1967 introduced the method of combining the output signals from two opposing detectors in area scanning in order to achieve a uniform sensitivity independent of the depth of the source in the body. Arimizu et al. (60, 90) and Sharma (58) reported that the geometric mean of the counts from two opposed detectors yielded a better estimation of organ counts irrespective of the depth of the source than did the simple arithmetic mean of the counts. Arimizu and Morris (60) felt, however, that for ^{99m}Tc the average of the arithmetic and geometric means was an even better approximation. Since the value of using the geometric mean has been noted by other researchers (57, 91) an experiment was performed to determine whether the geometric or arithmetic mean alone or their average would serve as the best approximation for our experimental arrangement.

A rectangular plexiglass volume phantom [20 x 13 x 8 cm] and an Alderson kidney phantom were placed in turn in a plexiglass water bath [37 x 37 x 30 cm] filled to a depth of 25 cm. The rectilinear scanner, as described in Chapter IV, scanned each phantom at 7 to 8 different depths in the water bath with the upper detector 34.5 cm and the lower

detector 1.5 cm from the top of the scan table and the following scanner settings:

[1] scan speed	250 cm/min
[2] longitudinal speed	750 cm/min
[3] centerline	140 keV
[4] window	± 20 keV
[5] line spacing	0.25 inches

The anti-scattering and smoothing routines mentioned in Chapter V were used to define the phantom border and the "raw" counts within these borders were determined for each detector. After correction for background and radioactive decay, the arithmetic mean, 1/2 [upper detector counts + lower detector counts], and the geometric mean, [upper detector counts x lower detector counts]$^{1/2}$ were determined for each scan. The results, expressed as % of 30,000 and 11,430 counts for the volume and kidney phantoms respectively, were plotted against source center displacement from the center of the water bath.

Figure A-2 illustrates the results using the volume phantom. When the center of the volume phantom was displaced 7 cm to either side of the water bath center the arithmetic mean increased to 135% and 150% at the maximum displacement positions while the geometric mean decreased to only 94% and 93%. The results from the kidney phantom are shown in Figure A-3. With the same displacement as the volume phantom, the arithmetic mean of the kidney counts increased to 152% and 167% at each extreme while the geometric mean decreased to 84% and 90%.

It was concluded that the geometric mean showed less count variation as the source depth changed than did the arithmetic mean and that the average of the two means would yield no improvement.

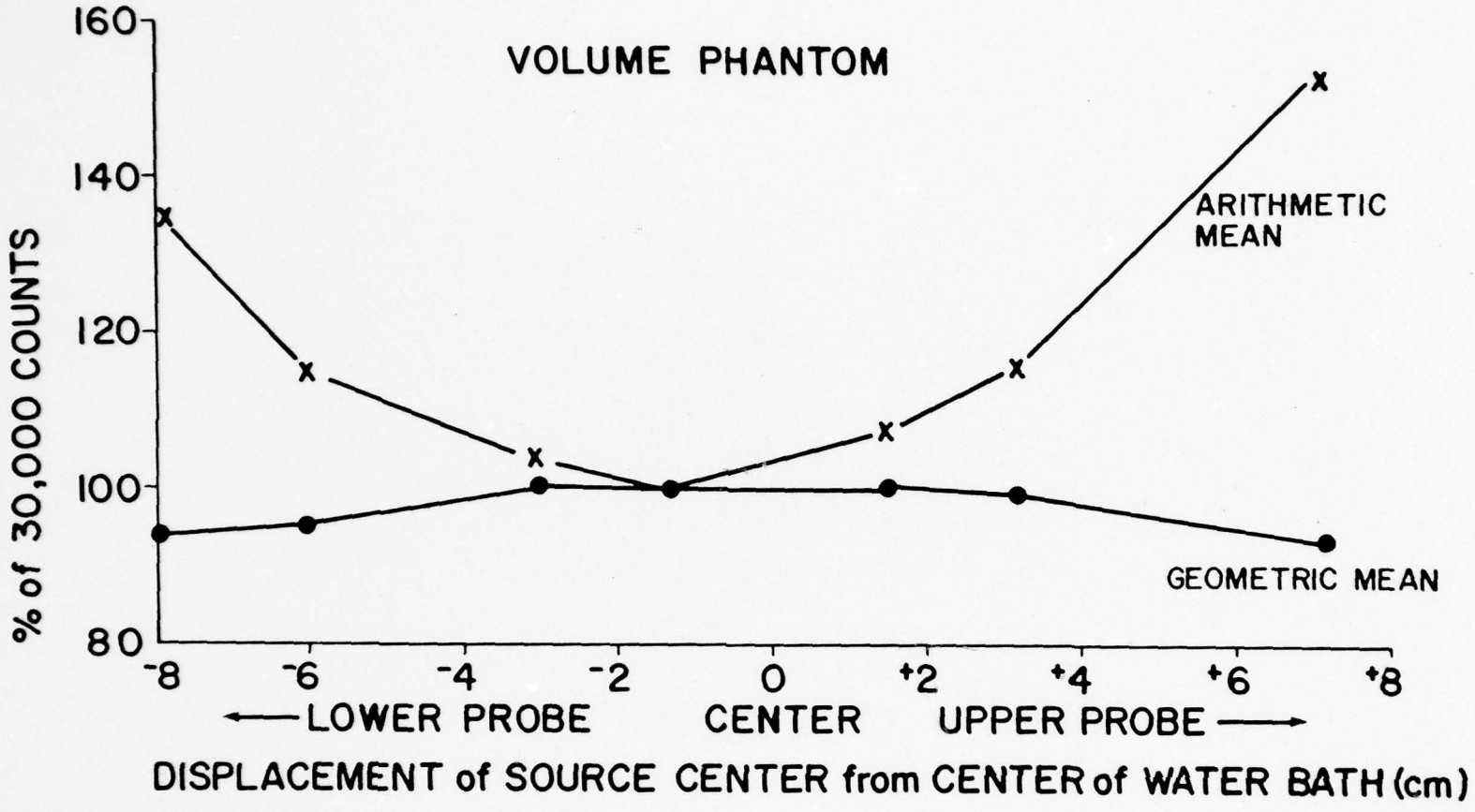

FIGURE A-2

Variation of the arithmetic and geometric means with source depth variation [volume phantom].

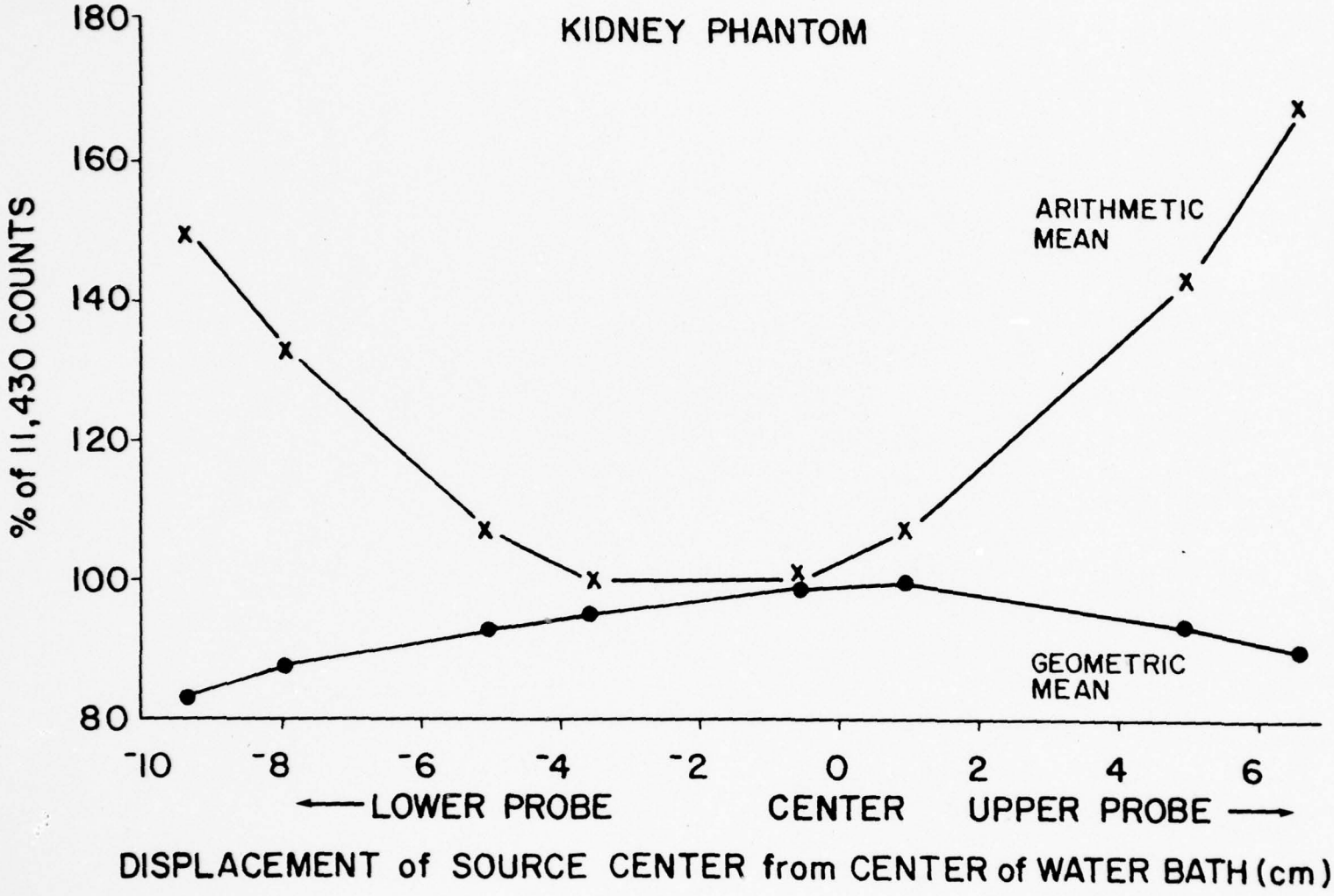

FIGURE A-3

Variation of the arithmetic and geometric means with source depth variation [kidney phantom].

APPENDIX 3

CLINICAL STATUS OF PATIENT-VOLUNTEERS

TABLE A-1

CLINICAL STATUS OF PATIENT VOLUNTEERS

Study #	Patient #	Height (cm)	Weight (kg)	Body Surface Area (m^2)*	Liver Weight** (kg)	Chest Thickness*** (cm)	Waist Thickness (cm)
9	7445	162.6	44.00	1.438	1.247	22	18
10	5586	186.1	83.01	2.078	1.899	23	24
11	8218	168.3	67.59	1.770	1.585	23	22
12	1655	170.2	68.95	1.800	1.1616	24	24
13	2773	173.4	57.61	1.690	1.504	24	18
14	8228	179.1	67.59	1.852	1.669	23	22
15	2190	170.2	63.50	1.738	1.553	26	24
16	3245	179.1	88.00	2.071	1.893	28	27
17	9319	167.6	58.06	1.654	1.467	22	21
18	9367	171.4	53.52	1.624	1.437	23	19
19	8163	165.1	58.97	1.647	1.460	22	22
20	8914	172.7	49.90	1.585	1.397	18	18
21	6730	180.3	72.58	1.912	1.730	22	22
22	2470	173.4	81.65	1.960	1.779	24	24
23	8164	175.9	77.57	1.938	1.757	23	23
24	4193	168.9	67.13	1.769	1.585	22	21
26	1670	153.7	66.68	1.648	1.461	23	27
27	6082	168.9	56.70	1.647	1.460	20	18
28	1337	179.1	92.08	2.112	1.934	28	29
INDIVIDUAL AVERAGE		171.9	67.11	1.786	1.602	23.4	22.5
INDIVIDUAL RANGE		154-186	44-92	1.4-2.1	1.2-1.9	18-28	18-29

*(92-93)
**(94)
***Anterior-posterior thickness

TABLE A-1 (Continued)

Study #	Patient #	Age	Race	Distance of Upper Probe from Table Top*	Amount Injected (mCi)	# of Scan Images	Health Description
9	7445	60	N	27.0	3.99	10	LUL Nodule, degenerative arthritis
10	5586	30	N	29.0	3.97	10	Hemochromatosis, anemia
11	8218	43	N	28.4	3.98	9	basal cell CA nose
12	1655	66	C	28.5	4.23	3	Pancreatitis
13	2773	63	C	27.0	3.70	5	LUL Lesion
14	8228	53	C	28.0	3.91	9	Choledochoenterostomy**
15	2190	75	C	28.8	3.60	7	CA Lung
16	3245	48	C	30.0	4.04	8	Polychthemia
17	9319	62	N	28.0	3.82	5	Adenocarcinoma Lung
18	9367		C	26.0	3.84	8	Possible CA Lung
19	8163	64	C	26.6	3.86	7	CA Lung
20	8914	51	N	26.0	3.92	7	T B
21	6730	49	C	28.5	4.09	7	LUL Lesion
22	2470	49	N	31.0	3.89	7	Pulmonary Hypertension
23	8164	51	N	29.0	3.89	6	Pulmonary Hypertension
24	4193	47	N	27.5	4.17	7	Abdominal discomfort
26	1670	69	C	31.0	3.69	8	Superficial Stomach Ulcer
27	6082	55	C	28.0	3.84	4	CA Lung, severe weight loss
28	1337	55	C	30.5	4.13	6	Splenomegaly, gallstones
AVERAGE		55		28.5	3.92	7	
RANGE		30-75		26-31		3-10	

*Lower probe was a constant 1.5 cm from table top
**Also had liver lesion

APPENDIX 4

CUMULATED ACTIVITY AND ABSORBED DOSE VALUES
I. GEOMETRIC MEAN DATA

AD-A044 624 AIR FORCE INST OF TECH WRIGHT-PATTERSON AFB OHIO F/G 6/18
RADIATION DOSE TO HUMANS FROM 99M TC LABELED DIHYDROTHIOCTIC AC--ETC(U)
1976 K N VANEK

UNCLASSIFIED AFIT-CI-77-14 NL

2 OF 2
AD
A044624

END
DATE
FILMED
10-77
DDC

TABLE A-2

CUMULATED ACTIVITY* (μCi-hrs/mCi administered)

I. GEOMETRIC MEAN DATA

Study #	Patient #	Liver	Kidneys	Intestines	Blood**
9	7445	1803	305	1092	2002
10	5586	1065	350	502	"
11	8218	1152	108	601	"
12	1655	933	237	592	"
13	2773	1922	408	1183	"
14	8228	2250	220	795	"
15	2190	1055	439	963	"
16	3245	1310	182	747	"
17	9319	1198	480	542	"
18	9367	1404	520	1287	"
19	8163	863	205	754	"
20	8914	826	810	792	"
21	6730	1303	414	1310	"
22	2470	1328	151	391	"
23	8164	1080	202	830	"
24	4193	1349	409	937	"
26	1670	1140	384	723	"
27	6082	1192	511	729	"
28	1337	1008	354	849	"
COMBINED DATA		1307	317	878	2002
INDIVIDUAL AVERAGE		1273	352	822	N/A
INDIVIDUAL RANGE		825-2250	108-810	391-1310	N/A

*Assumes physical decay only after the last datum point.
**Blood value based on a combined data curve only.

TABLE A-3

ABSORBED DOSE (mrads/mCi administered) FROM ^{99m}Tc-DHTA

I. GEOMETRIC MEAN DATA

Study #	Patient #	Liver	Kidneys	Intestines	Ovaries	Testes	Red Marrow
9	7445	90	73	68	19	4.0	14
10	5586	56	76	35	12	3.7	11
11	8218	59	31	40	13	3.8	11
12	1655	49	55	39	13	3.8	11
13	2773	96	93	73	20	4.1	16
14	8228	110	57	52	16	3.9	14
15	2190	56	95	60	17	3.9	13
16	3245	67	46	48	14	3.8	12
17	9319	62	102	38	12	3.8	12
18	9367	73	112	79	21	4.1	16
19	8163	46	49	48	14	3.8	11
20	8914	47	164	52	16	3.9	14
21	6730	68	92	79	21	4.1	15
22	2470	67	39	29	10	3.7	10
23	8164	56	49	52	15	3.9	12
24	4193	70	90	59	17	4.0	14
26	1670	60	84	47	14	3.8	12
27	6082	62	108	48	14	3.8	13
28	1337	54	78	54	16	3.9	12
COMBINED DATA		67	72	56	16	3.9	13
INDIVIDUAL AVERAGE		66	79	53	16	3.9	13
INDIVIDUAL RANGE		46-110	31-164	29-79	10-21	3.7-4.1	10-16

TABLE A-4

ABSORBED DOSE (mrads/mCi administered) TO THE LIVER

I. GEOMETRIC MEAN DATA

Study #	Patient #	Liver	Kidneys	Intestines	Blood	Total
9	7445	83	1.2	1.9	4.4	90.4
10	5586	49	1.4	0.9	"	55.7
11	8218	53	0.4	1.1	"	58.9
12	1655	43	0.9	1.0	"	49.3
13	2773	88	1.6	2.1	"	96.5
14	8228	103	0.9	1.4	"	110.0
15	2190	48	1.7	1.7	"	56.3
16	3245	60	0.7	1.3	"	66.7
17	9319	55	1.9	1.0	"	62.4
18	9367	65	2.0	2.3	"	73.3
19	8163	40	0.8	1.3	"	46.2
20	8914	38	3.2	1.4	"	46.9
21	6730	60	1.6	2.3	"	68.2
22	2470	61	0.6	0.7	"	66.8
23	8164	50	0.8	1.5	"	56.3
24	4193	62	1.6	1.6	"	69.7
26	1670	52	1.5	1.3	"	59.6
27	6082	55	2.0	1.3	"	62.5
28	1337	46	1.4	1.5	"	53.6
COMBINED DATA		60	1.2	1.6	4.4	67.3
INDIVIDUAL AVERAGE		58	1.4	1.5	N/A	65.8
INDIVIDUAL RANGE		38-103	0.4-3.2	0.7-2.3	N/A	46-110

TABLE A-5

ABSORBED DOSE (mrads/mCi administered) TO THE KIDNEYS

I. GEOMETRIC MEAN DATA

Study #	Patient #	Liver	Kidneys	Intestines	Blood	Total
9	7445	7.0	58.0	3.2	4.4	72.6
10	5586	4.2	66.4	1.5	"	76.4
11	8218	4.5	20.5	1.8	"	31.2
12	1655	3.6	45.1	1.7	"	54.9
13	2773	7.5	77.5	3.4	"	92.9
14	8228	8.8	41.7	2.3	"	57.2
15	2190	4.1	83.5	2.8	"	94.8
16	3245	5.1	34.7	2.2	"	46.3
17	9319	4.7	91.2	1.6	"	102.0
18	9367	5.5	98.8	3.8	"	112.0
19	8163	3.4	38.9	2.2	"	48.9
20	8914	3.2	154.0	2.3	"	164.0
21	6730	5.1	78.8	3.8	"	92.1
22	2470	5.2	28.7	1.1	"	39.4
23	8164	4.2	38.5	2.4	"	49.5
24	4193	5.3	77.7	2.7	"	90.1
26	1670	4.4	73.0	2.1	"	84.0
27	6082	4.6	97.1	2.1	"	108.0
28	1337	3.9	67.3	2.5	"	78.1
COMBINED DATA		5.1	60.2	2.6	4.4	72.3
INDIVIDUAL AVERAGE		5.0	66.9	2.4	N/A	78.7
INDIVIDUAL RANGE		3.2-8.8	20-154	1.1-3.8	N/A	31-164

TABLE A-6

ABSORBED DOSE (mrads/mCi administered) TO THE INTESTINES

I. GEOMETRIC MEAN DATA

Study #	Patient #	Liver	Kidneys	Intestines	Blood	Total
9	7445	2.8	0.8	59.4	4.9	68.0
10	5586	1.7	0.9	27.3	"	34.9
11	8218	1.8	0.3	32.7	"	39.7
12	1655	1.5	0.6	32.2	"	39.2
13	2773	3.0	1.1	64.4	"	73.4
14	8228	3.6	0.6	43.3	"	52.3
15	2190	1.7	1.2	52.4	"	60.2
16	3245	2.1	0.5	40.7	"	48.1
17	9319	1.9	1.3	29.5	"	37.6
18	9367	2.2	1.4	70.0	"	78.6
19	8163	1.4	0.5	41.0	"	47.9
20	8914	1.3	2.2	43.1	"	51.5
21	6730	2.1	1.1	71.3	"	79.4
22	2470	2.1	0.4	21.3	"	28.7
23	8164	1.7	0.5	45.2	"	52.4
24	4193	2.1	1.1	51.0	"	59.1
26	1670	1.8	1.0	39.3	"	47.1
27	6082	1.9	1.4	39.7	"	47.8
28	1337	1.6	0.9	46.2	"	53.6
COMBINED DATA		2.1	0.8	47.8	4.9	55.6
INDIVIDUAL AVERAGE		2.0	0.9	44.7	N/A	52.6
INDIVIDUAL RANGE		1.3-3.6	0.3-2.2	21-71	N/A	29-79

TABLE A-7

ABSORBED DOSE (mrads/mCi administered) TO THE OVARIES

I. GEOMETRIC MEAN DATA

Study #	Patient #	Liver	Kidneys	Intestines	Blood	Total
9	7445	0.8	0.3	12.9	4.8	18.9
10	5586	0.5	0.4	5.9	"	11.6
11	8218	0.5	0.1	7.1	"	12.6
12	1655	0.4	0.3	7.0	"	12.5
13	2773	0.9	0.4	14.0	"	20.1
14	8228	1.0	0.2	9.4	"	15.5
15	2190	0.5	0.5	11.4	"	17.2
16	3245	0.6	0.2	8.8	"	14.4
17	9319	0.5	0.5	6.4	"	12.3
18	9367	0.6	0.6	15.2	"	21.2
19	8163	0.4	0.2	8.9	"	14.3
20	8914	0.4	0.9	9.4	"	15.5
21	6730	0.6	0.5	15.5	"	21.4
22	2470	0.6	0.2	4.6	"	10.2
23	8164	0.5	0.2	9.8	"	15.3
24	4193	0.6	0.4	11.1	"	17.0
26	1670	0.5	0.4	8.6	"	14.3
27	6082	0.5	0.6	8.6	"	14.5
28	1337	0.4	0.4	10.0	"	15.7
COMBINED DATA		0.6	0.4	10.4	4.8	16.1
INDIVIDUAL AVERAGE		0.6	0.4	9.7	N/A	15.5
INDIVIDUAL RANGE		0.4-1.0	0.1-0.9	5-16	N/A	10-21

TABLE A-8

ABSORBED DOSE (mrads/mCi administered) TO THE TESTES

I. GEOMETRIC MEAN DATA

Study #	Patient #	Liver	Kidneys	Intestines	Blood	Total
9	7445	0.11	0.03	0.49	3.40	4.04
10	5586	0.07	0.04	0.23	"	3.73
11	8218	0.07	0.01	0.27	"	3.76
12	1655	0.06	0.02	0.27	"	3.75
13	2773	0.12	0.04	0.54	"	4.09
14	8228	0.14	0.02	0.36	"	3.92
15	2190	0.06	0.04	0.44	"	3.94
16	3245	0.08	0.02	0.34	"	3.84
17	9319	0.07	0.04	0.24	"	3.77
18	9367	0.09	0.05	0.58	"	4.12
19	8163	0.05	0.02	0.34	"	3.82
20	8914	0.05	0.07	0.36	"	3.88
21	6730	0.08	0.04	0.59	"	4.11
22	2470	0.08	0.01	0.18	"	3.68
23	8164	0.07	0.02	0.38	"	3.86
24	4193	0.08	0.04	0.42	"	3.95
26	1670	0.07	0.03	0.33	"	3.83
27	6082	0.07	0.04	0.33	"	3.85
28	1337	0.06	0.03	0.38	"	3.88
COMBINED DATA		0.08	0.03	0.40	3.40	3.91
INDIVIDUAL AVERAGE		0.08	0.03	0.37	N/A	3.89
INDIVIDUAL RANGE		0.05-0.14	0.01-0.07	0.2-0.6	N/A	3.7-4.1

TABLE A-9

ABSORBED DOSE (mrads/mCi administered) TO THE RED MARROW

I. GEOMETRIC MEAN DATA

Study #	Patient #	Liver	Kidneys	Intestines	Blood	Total
9	7445	2.88	1.16	4.69	5.81	14.5
10	5586	1.70	1.33	2.16	"	11.0
11	8218	1.84	0.41	2.58	"	10.6
12	1655	1.49	0.90	2.54	"	10.7
13	2773	3.08	1.55	5.08	"	15.5
14	8228	3.60	0.83	3.41	"	13.7
15	2190	1.69	1.67	4.14	"	13.3
16	3245	2.10	0.69	3.21	"	11.8
17	9319	1.92	1.82	2.33	"	11.9
18	9367	2.25	1.98	5.52	"	15.6
19	8163	1.38	0.78	3.24	"	11.2
20	8914	1.32	3.08	3.40	"	13.6
21	6730	2.08	1.58	5.62	"	15.1
22	2470	2.12	0.57	1.68	"	10.2
23	8164	1.73	0.77	3.56	"	11.9
24	4193	2.16	1.55	4.02	"	13.5
26	1670	1.82	1.46	3.10	"	12.2
27	6082	1.91	1.94	3.13	"	12.8
28	1337	1.61	1.35	3.64	"	12.4
COMBINED DATA		2.09	1.20	3.77	5.81	12.9
INDIVIDUAL AVERAGE		2.04	1.34	3.53	N/A	12.7
INDIVIDUAL RANGE		1.3-3.6	0.4-3.1	1.7-5.6	N/A	10-16

APPENDIX 5

CUMULATED ACTIVITY AND ABSORBED DOSE VALUES
II. ARITHMETIC MEAN DATA

TABLE A-10

CUMULATED ACTIVITY* (μCi-hrs/mCi administered)

II. ARITHMETIC MEAN DATA

Study #	Patient #	Liver	Kidneys	Intestines	Blood**
9	7445	1908	316	1109	2002
10	5586	1087	376	546	"
11	8218	1168	126	650	"
12	1655	940	251	599	"
13	2773	1984	416	1234	"
14	8228	2263	238	825	"
15	2190	1077	451	982	"
16	3245	1317	189	797	"
17	9319	1225	511	556	"
18	9367	1443	529	1334	"
19	8163	889	218	785	"
20	8914	846	832	807	"
21	6730	1333	488	1385	"
22	2470	1366	154	407	"
23	8164	1116	211	897	"
24	4193	1401	412	1003	"
26	1670	1166	418	792	"
27	6082	1306	557	767	"
28	1337	1012	378	942	"
COMBINED DATA		1345	333	927	2002
INDIVIDUAL AVERAGE		1308	372	864	N/A
INDIVIDUAL RANGE		846-2263	126-831	407-1385	N/A

*Assumes physical decay only after the last datum point.
**Blood value based on a combined data curve only.

TABLE A-11

ABSORBED DOSE (mrads/mCi administered) FROM ^{99m}Tc-DHTA

II. ARITHMETIC MEAN DATA

Study #	Patient #	Liver	Kidneys	Intestines	Ovaries	Testes	Red Marrow
9	7445	95	75	69	19	4.0	15
10	5586	56	82	37	12	3.8	11
11	8218	60	35	42	13	3.8	11
12	1655	50	57	40	13	3.8	11
13	2773	100	95	76	21	4.1	16
14	8228	111	61	54	16	3.9	14
15	2190	57	97	61	17	4.0	14
16	3245	67	48	51	15	3.9	12
17	9319	64	108	38	12	3.8	12
18	9367	75	114	81	22	4.1	16
19	8163	48	52	50	15	3.8	11
20	8914	48	168	52	16	3.9	14
21	6730	70	106	84	22	4.2	16
22	2470	69	40	30	10	3.7	11
23	8164	58	51	56	16	3.9	12
24	4193	72	91	63	18	4.0	14
26	1670	61	91	51	15	3.9	13
27	6082	68	117	50	15	3.9	13
28	1337	54	83	59	17	3.9	13
COMBINED DATA		69	76	58	17	3.9	13
INDIVIDUAL AVERAGE		67	83	55	16	3.9	13
INDIVIDUAL RANGE		48-111	35-168	30-84	10-22	3.7-4.1	11-16

TABLE A-12

ABSORBED DOSE (mrads/mCi administered) TO THE LIVER

II. ARITHMETIC MEAN DATA

Study #	Patient #	Liver	Kidneys	Intestines	Blood	Total
9	7445	87.8	1.2	2.0	4.4	95.3
10	5586	50.0	1.5	1.0	"	56.8
11	8218	53.7	0.5	1.2	"	59.8
12	1655	43.3	1.0	1.1	"	49.7
13	2773	91.3	1.6	2.2	"	99.5
14	8228	104.0	0.9	1.4	"	111.0
15	2190	49.5	1.8	1.7	"	57.4
16	3245	60.6	0.7	1.4	"	67.1
17	9319	56.4	2.0	1.0	"	63.7
18	9367	66.4	2.1	2.4	"	75.2
19	8163	40.9	0.8	1.4	"	47.6
20	8914	38.9	3.2	1.4	"	48.0
21	6730	61.3	1.9	2.4	"	70.1
22	2470	62.8	0.6	0.7	"	68.6
23	8164	51.3	0.8	1.6	"	58.1
24	4193	64.4	1.6	1.8	"	72.2
26	1670	53.6	1.6	1.4	"	61.1
27	6082	60.1	2.2	1.4	"	68.0
28	1337	46.6	1.5	1.7	"	54.1
COMBINED DATA		61.9	1.3	1.6	4.4	69.2
INDIVIDUAL AVERAGE		60.2	1.4	1.5	N/A	67.5
INDIVIDUAL RANGE		39-104	0.5-3.2	0.7-2.3	N/A	48-111

TABLE A-13

ABSORBED DOSE (mrads/mCi administered) TO THE KIDNEYS

II. ARITHMETIC MEAN DATA

Study #	Patient #	Liver	Kidneys	Intestines	Blood	Total
9	7445	7.4	60.0	3.2	4.4	75.1
10	5586	4.2	71.4	1.6	"	81.6
11	8218	4.6	23.9	1.9	"	34.7
12	1655	3.7	47.6	1.7	"	57.4
13	2773	7.7	79.0	3.6	"	94.8
14	8228	8.8	45.3	2.4	"	60.9
15	2190	4.2	85.6	2.9	"	97.1
16	3245	5.1	35.8	2.3	"	47.7
17	9319	4.8	97.0	1.6	"	108.0
18	9367	5.6	100.0	3.9	"	114.0
19	8163	3.5	41.4	2.3	"	51.6
20	8914	3.3	158.0	2.4	"	168.0
21	6730	5.2	92.7	4.0	"	106.0
22	2470	5.3	29.2	1.2	"	40.1
23	8164	4.4	40.0	2.6	"	51.4
24	4193	5.5	78.2	2.9	"	91.0
26	1670	4.6	79.3	2.3	"	90.6
27	6082	5.1	106.0	2.2	"	117.0
28	1337	4.0	71.8	2.7	"	82.9
COMBINED DATA		5.2	63.2	2.7	4.4	75.5
INDIVIDUAL AVERAGE		5.1	70.6	2.5	N/A	82.6
INDIVIDUAL RANGE		3.3-8.8	24-158	1.2-3.9	N/A	35-168

TABLE A-14

ABSORBED DOSE (mrads/mCi administered) TO THE INTESTINES

II. ARITHMETIC MEAN DATA

Study #	Patient #	Liver	Kidneys	Intestines	Blood	Total
9	7445	3.1	0.8	60.4	4.9	69.1
10	5586	1.7	1.0	29.7	"	37.3
11	8218	1.8	0.3	35.4	"	42.5
12	1655	1.5	0.7	32.6	"	39.7
13	2773	3.1	1.1	67.2	"	76.3
14	8228	3.6	0.7	44.9	"	54.0
15	2190	1.7	1.2	53.5	"	61.3
16	3245	2.1	0.5	43.4	"	50.9
17	9319	1.9	1.4	30.2	"	38.5
18	9367	2.3	1.4	72.6	"	81.2
19	8163	1.4	0.6	42.7	"	49.7
20	8914	1.3	2.2	43.9	"	52.4
21	6730	2.1	1.3	75.4	"	83.7
22	2470	2.2	0.4	22.2	"	29.7
23	8164	1.8	0.6	48.8	"	56.1
24	4193	2.2	1.1	54.6	"	62.8
26	1670	1.8	1.1	73.1	"	51.0
27	6082	2.1	1.5	41.7	"	50.2
28	1337	1.6	1.0	51.3	"	58.8
COMBINED DATA		2.1	0.9	50.4	"	58.4
INDIVIDUAL AVERAGE		2.1	1.0	47.0	N/A	55.0
INDIVIDUAL RANGE		1.3-3.6	0.3-2.2	22-75	N/A	30-84

TABLE A-15

ABSORBED DOSE (mrads/mCi administered) TO THE OVARIES

II. ARITHMETIC MEAN DATA

Study #	Patient #	Liver	Kidneys	Intestines	Blood	Total
9	7445	0.9	0.4	13.1	4.8	19.1
10	5586	0.5	0.4	6.5	"	12.2
11	8218	0.5	0.1	7.7	"	13.2
12	1655	0.4	0.3	7.1	"	12.6
13	2773	0.9	0.5	14.6	"	20.8
14	8228	1.0	0.3	9.8	"	15.9
15	2190	0.5	0.5	11.6	"	17.4
16	3245	0.6	0.2	9.4	"	15.0
17	9319	0.6	0.6	6.6	"	12.5
18	9367	0.7	0.6	15.8	"	21.8
19	8163	0.4	0.2	9.3	"	14.7
20	8914	0.4	0.9	9.6	"	15.7
21	6730	0.6	0.5	16.4	"	22.3
22	2470	0.6	0.2	4.8	"	10.4
23	8164	0.5	0.2	10.6	"	16.2
24	4193	0.6	0.4	11.9	"	17.8
26	1670	0.5	0.5	9.4	"	15.2
27	6082	0.6	0.6	9.1	"	15.1
28	1337	0.5	0.4	11.2	"	16.8
COMBINED DATA		0.6	0.4	11.0	4.8	16.7
INDIVIDUAL AVERAGE		0.6	0.4	10.2	N/A	16.0
INDIVIDUAL RANGE		0.4-1.0	0.1-0.9	5-16	N/A	10-22

TABLE A-16

ABSORBED DOSE (mrads/mCi administered) TO THE TESTES

II. ARITHMETIC MEAN DATA

Study #	Patient #	Liver	Kidneys	Intestines	Blood	Total
9	7445	0.12	0.03	0.50	3.40	4.05
10	5586	0.07	0.03	0.25	"	3.75
11	8218	0.07	0.01	0.29	"	3.78
12	1655	0.06	0.02	0.27	"	3.75
13	2773	0.12	0.04	0.56	"	4.12
14	8228	0.14	0.02	0.37	"	3.94
15	2190	0.07	0.04	0.44	"	3.95
16	3245	0.08	0.02	0.36	"	3.86
17	9319	0.08	0.04	0.25	"	3.78
18	9367	0.09	0.05	0.60	"	4.14
19	8163	0.06	0.02	0.35	"	3.83
20	8914	0.05	0.07	0.36	"	3.89
21	6730	0.08	0.04	0.63	"	4.16
22	2470	0.08	0.01	0.18	"	3.69
23	8164	0.07	0.02	0.41	"	3.90
24	4193	0.09	0.04	0.45	"	3.98
26	1670	0.07	0.04	0.36	"	3.87
27	6082	0.08	0.05	0.35	"	3.88
28	1337	0.06	0.03	0.43	"	3.93
COMBINED DATA		0.08	0.03	0.42	3.40	3.94
INDIVIDUAL AVERAGE		0.08	0.03	0.39	N/A	3.90
INDIVIDUAL RANGE		0.05-0.14	0.01-0.07	0.2-0.6	N/A	3.7-4.1

TABLE A-17

ABSORBED DOSE (mrads/mCi administered) TO THE RED MARROW

II. ARITHMETIC MEAN DATA

Study #	Patient #	Liver	Kidneys	Intestines	Blood	Total
9	7445	3.05	1.20	4.76	5.81	14.8
10	5586	1.74	1.43	2.34	"	11.3
11	8218	1.87	0.48	2.79	"	10.9
12	1655	1.50	0.95	2.57	"	10.8
13	2773	3.17	1.58	5.30	"	15.9
14	8228	3.62	0.90	3.54	"	13.9
15	2190	1.72	1.71	4.22	"	13.5
16	3245	2.11	0.72	3.42	"	12.1
17	9319	1.96	1.94	2.39	"	12.1
18	9367	2.31	2.01	5.72	"	15.8
19	8163	1.42	0.83	3.37	"	11.4
20	8914	1.35	3.16	3.46	"	13.8
21	6730	2.13	1.85	5.94	"	15.7
22	2470	2.19	0.58	1.75	"	10.3
23	8164	1.79	0.80	3.85	"	12.2
24	4193	2.24	1.56	4.31	"	13.9
26	1670	1.87	1.59	3.40	"	12.7
27	6082	2.09	2.12	3.29	"	13.3
28	1337	1.62	1.44	4.04	"	12.9
COMBINED DATA		2.15	1.26	3.98	5.81	13.2
INDIVIDUAL AVERAGE		2.09	1.39	3.71	N/A	13.0
INDIVIDUAL RANGE		1.4-3.6	0.5-3.2	1.8-5.9	N/A	11-16

APPENDIX 6

A COMPARISON OF ABSORBED RADIATION DOSE USING THE GEOMETRIC AND ARITHMETIC MEAN DATA

The value of using the geometric mean of the counts from two opposed detectors instead of the arithmetic mean for quantitative measurment of radioactivity in internal organs by area scanning has already been discussed in Appendix 2. Thus far, discussion has been limited to the effects that the two means had upon recorded counts. Absorbed radiation dose estimates using both means are presented in TABLES A-18 through A-23, together with the % increases which occurred with the arithmetic mean data.

Except for the kidneys, the % increases in the dose estimates that occurred when the arithmetic means rather than the geometric means were used were equal to or less than 10%. With the kidneys [TABLE A-19], only 2 of 19 patients exceeded this 10% limit [12.9% and 15.2%]. The variation in the individual average and the combined data study was less than 6% for all target organs.

When attempting to assess the value of using the geometric mean instead of the simpler arithmetic mean, one must consider the source organ in question. Large massive organs such as the liver and intestinal area will exhibit only slight variations between the two means due to the relatively minor depth changes within the patient. Smaller organs such as the kidneys, not only may have greater depth variation, but maybe situated closer to one detector than the other [e.g. the kidneys are closer

to the posterior detector] thus showing a greater difference between the two means [see Appendix 2].

In the case where a target organ is not a source organ, the effect of the different means may be estimated by noting their effect upon the major contributing source organ. For example, the major contributor to the absorbed radiation dose to the testes is the blood [see Appendix 4 and 5]. The cumulated activity for the blood was the same for both situations, since blood activity was determined using a well counter, therefore resulting in minor variations in the testes dose estimates. As seen in TABLE A-22, the % increase only ranged from 0.0 to 2.7% with no differences between the combined data study or individual average. The major contributor to the ovaries dose was the intestinal area [see Appendix 4 and 5] and similar variations in the % increase exist for the intestinal area and ovaries. The % increase for the ovaries range from 0.0 to 7.1% and from 0.0 to 8.5% for the intestines [TABLES A-20 and A-21 respectively]. The combined data study showed a 3.6% difference in the means for the intestines and 6.2% for the ovaries, while the individual average differences were 4.4% and 0.0% respectively.

Thus, when attempting to determine whether the geometric mean or the arithmetic mean of the counts from opposed detectors should be used to estimate absorbed radiation doses, one should consider the size of the source organ, its location with respect to the central axis of the body, its potential depth variance, the major dose contributors to the target organs, and the impact that a 10% dose variation may have upon final data analysis. With the scarcity of quantitative <u>in vivo</u> data, the inability to obtain the geometric mean of the counts from opposed detectors should not deter one from using data based on the arithmetic mean.

TABLE A-18

COMPARISON OF ARITHMETIC MEAN AND GEOMETRIC MEAN DOSE ESTIMATES
(mrads/mCi administered)

LIVER

Study #	Patient #	Geometric	Arithmetic	% Increase*
9	7445	90	95	5.6
10	5586	56	56	0.0
11	8218	59	60	1.7
12	1655	49	50	2.0
13	2773	96	100	4.2
14	8228	110	111	0.9
15	2190	56	57	1.8
16	3245	67	67	0.0
17	9319	62	64	3.2
18	9367	73	75	2.7
19	8163	46	48	4.3
20	8914	47	48	2.1
21	6730	68	70	2.9
22	2470	67	69	3.0
23	8164	56	58	3.6
24	4193	70	72	2.9
26	1670	60	61	1.7
27	6082	62	68	9.7
28	1337	54	54	0.0
COMBINED		67	69	3.0
INDIVIDUAL AVERAGE		66	67	1.5
RANGE		46-110	48-111	0.0-9.7

*% Increase above geometric mean

TABLE A-19

COMPARISON OF ARITHMETIC MEAN AND GEOMETRIC MEAN DOSE ESTIMATES
(mrads/mCi administered)

KIDNEYS

Study #	Patient #	Geometric	Arithmetic	% Increase*
9	7445	73	75	2.7
10	5586	76	82	7.9
11	8218	31	35	12.9
12	1655	55	57	3.6
13	2773	93	95	2.2
14	8228	57	61	7.0
15	2190	95	97	2.1
16	3245	46	48	4.3
17	9319	102	108	5.9
18	9367	112	114	1.8
19	8163	49	52	6.1
20	8914	164	168	2.4
21	6730	92	106	15.2
22	2470	39	40	2.6
23	8164	49	51	4.1
24	4193	90	91	1.1
26	1670	84	91	8.3
27	6082	108	117	8.3
28	1337	78	83	6.4
COMBINED		72	76	5.6
INDIVIDUAL AVERAGE		79	83	5.5
RANGE		31-164	35-168	1.1-15.2

*% Increase above geometric mean

TABLE A-20

COMPARISON OF ARITHMETIC MEAN AND GEOMETRIC MEAN DOSE ESTIMATES
(mrads/mCi administered)

INTESTINES

Study #	Patient #	Geometric	Arithmetic	% Increase*
9	7445	68	69	1.5
10	5586	35	37	5.7
11	8218	40	42	5.0
12	1655	39	40	2.6
13	2773	73	76	4.1
14	8288	52	54	3.8
15	2190	60	61	1.7
16	3245	48	51	6.2
17	9319	38	38	0.0
18	9367	79	81	2.5
19	8163	48	50	4.2
20	8914	52	52	0.0
21	6730	79	84	6.3
22	2470	29	30	3.4
23	8164	52	56	7.7
24	4193	59	63	6.8
26	1670	47	51	8.5
27	6082	48	50	4.2
28	1337	54	59	9.3
COMBINED		56	58	3.6
INDIVIDUAL AVERAGE		53	55	4.4
RANGE		29-79	30-84	0.0-8.5

*% Increase above geometric mean

TABLE A-21

COMPARISON OF ARITHMETIC MEAN AND GEOMETRIC MEAN DOSE ESTIMATES
(mrads/mCi administered)

OVARIES

Study #	Patient #	Geometric	Arithmetic	% Increase*
9	7445	19	19	0.0
10	5586	12	12	0.0
11	8218	13	13	0.0
12	1655	13	13	0.0
13	2773	20	21	5.0
14	8228	16	16	0.0
15	2190	17	17	0.0
16	3245	14	15	7.1
17	9319	12	12	0.0
18	9367	21	22	4.8
19	8163	14	15	7.1
20	8914	16	16	0.0
21	6730	21	22	4.8
22	2470	10	10	0.0
23	8164	15	16	6.7
24	4193	17	18	5.9
26	1670	14	15	7.1
27	6082	14	15	7.1
28	1337	16	17	6.2
COMBINED		16	17	6.2
INDIVIDUAL AVERAGE		16	16	0.0
RANGE		10-21	10-22	0.0-7.1

*% Increase above geometric mean

TABLE A-22

COMPARISON OF ARITHMETIC MEAN AND GEOMETRIC MEAN DOSE ESTIMATES
(mrads/mCi administered)

TESTES

Study #	Patient #	Geometric	Arithmetic	% Increase*
9	7445	4.0	4.0	0.0
10	5586	3.7	3.8	2.7
11	8218	3.8	3.8	0.0
12	1655	3.8	3.8	0.0
13	2773	4.1	4.1	0.0
14	8228	3.9	3.9	0.0
15	2190	3.9	4.0	2.6
16	3245	3.8	3.9	2.6
17	9319	3.8	3.8	0.0
18	9367	4.1	4.1	0.0
19	8163	3.8	3.8	0.0
20	8914	3.9	3.9	0.0
21	6730	4.1	4.2	2.4
22	2470	3.7	3.7	0.0
23	8164	3.9	3.9	0.0
24	4193	4.0	4.0	0.0
26	1670	3.8	3.9	2.6
27	6082	3.8	3.9	2.6
28	1337	3.9	3.9	0.0
COMBINED		3.9	3.9	0.0
INDIVIDUAL AVERAGE		3.9	3.9	0.0
RANGE		3.7-4.1	3.7-4.1	0.0-2.7

*% Increase above geometric mean

TABLE A-23

COMPARISON OF ARITHMETIC MEAN AND GEOMETRIC MEAN DOSE ESTIMATES
(mrads/mCi administered)

RED MARROW

Study #	Patient #	Geometric	Arithmetic	% Increase*
9	7445	14	15	7.1
10	5586	11	11	0.0
11	8218	11	11	0.0
12	1655	11	11	0.0
13	2773	16	16	0.0
14	8228	14	14	0.0
15	2190	13	14	7.7
16	3245	12	12	0.0
17	9319	12	12	0.0
18	9367	16	16	0.0
19	8163	11	11	0.0
20	8914	14	14	0.0
21	6730	15	16	6.7
22	2470	10	11	10.0
23	8164	12	12	0.0
24	4193	14	14	0.0
26	1670	12	13	8.3
27	6082	13	13	0.0
28	1337	12	13	8.3
COMBINED		13	13	0.0
INDIVIDUAL AVERAGE		13	13	0.0
RANGE		10-16	11-16	0.0-10

*% Increase above geometric mean

REFERENCES

1. Smith EM: General considerations in calculation of the absorbed dose of radiopharmaceuticals used in nuclear medicine. In Medical Radionuclides-Radiation Dose and Effects, Cloutier RJ, Edwards CL, Snyder WS, Eds., Oak Ridge, USAEC, 1970, pp 17-31.

2. Tonkin AK, DeLand FH: Dihydrothioctic acid, a new polygonal cell imaging agent. J Nucl Med 15:539, 1974.

3. Dugal P, Eikman A, Natarajan TK, et al: A quantitative test of gall bladder function. J Nucl Med 13:428, 1972.

4. Eikman EA, Cameron JL, Colman M, et al: Radioactive tracer techniques in the diagnosis of acute cholecystitis. J Nucl Med 14:393, 1973.

5. Eikman EA, Cameron JL, Colman M, et al: A test for patency of the cystic duct in acute cholecystitis. Ann Int Med 82:318-322, 1975.

6. 3M Company: Investigation of new drug report 9567, Attachment 6, St. Paul, Minn., 1973.

7. Netter FH: The CIBA Collection of Medical Illustrations, Vol 3, Part III, CIBA, pp 4-11.

8. Bloom W, Fawcett DW: A Textbook of Histology, 8th ed, Philadelphia, WB Saunders Company, 1962, pp 463-489.

9. Ham AW: Histology, 7th ed, Philadelphia, JB Lippincott Company, 1974, pp 686-714.

10. Root SW, Andrews GA, Kinsley RM, et al: The distribution and radiation effects of intravenously administered colloedal Au-198 in man. Cancer 7:856-866, 1954.

11. Sheppard CW, Wells EB, Hahn PF, et al: Studies of distribution of intravenously administered colloidal solutions of manganese dioxide and gold in human beings and dosages using radioactive isotopes. J Lab Clin Med 32:274-286, 1947.

12. Dobson EL, Jones HB: The behavior of intravenously injected particulate material. Acta Med Scand 144 (Suppl 243):1-71, 1952.

13. Stirrett LA, Yuhl ET: Clinical evaluation of hepatic radioactivity survey. Ann Surg 138:857-862, 1953.

14. Stirrett LA, Yuhl ET, Libby RL: A new technique for the diagnosis of carcinoma metastatic to the liver. Surg Gynec and Obst 96:210-214, 1953.

15. Stirrett LA, Yuhl ET, Cassen B: Clinical applications of hepatic radioactivity surveys. Amer J Gastroent 21:310-317, 1954.

16. Harper PV, Lathrop KA, Jiminez F, et al: Technetium 99m as a scanning agent. Radiology 85:101-109, 1965.

17. Goodwin DA, Stern HS, Wagner HN, et al: Indium-113m- a new radiopharmaceutical for liver scanning. Nucleonics 24:65,68, 1966.

18. Goodwin DA, Stern HS, Wagner HN, et al: Indium-113m- a new radiopharmaceutical for liver scanning. Nucleonics 24:65,68, 1966.

19. Sternlieb I, Scheingerg IH: Radiocopper in diagnosing liver disease. In Seminars in Nuclear Medicine, Vol II(2), Freeman LM, Blaufox MD, Eds., New York, Grune & Stratton, Inc., 1972, pp 176-188.

20. Yuhl ET, Stirrett LA, Hill MR, et al: The cholescintigram- a preliminary report. Surgery 34:724-727, 1953.

21. Taplin GM, Meredith OM, Kade H: The radioactive (I-131 tagged) rose bengal uptake excretion test for liver function using external gamma-ray scintillation counting techniques. J Lab Clin Med 45:665-678, 1955.

22. Rosenthall L: The Application of Radioiodinated Rose Bengal and Colloidal Radiogold in the Detection of Hepatobiliary Disease. St. Louis, Warren H. Green, Inc., 1969.

23. Friedell HL, MacIntyre WJ, Rejali AM: A method for the visualization of the configuration and structure of the liver. Am J Roentgen 77:455-470, 1957.

24. Johnston GS, Hupf HB, Gotshall E, et al: Zn-69m chloride, a new liver scanning agent. Amer J Roent 101:548-550, 1967.

25. Sorensen LB, Archambault M: Visualization of the liver by scanning with Mo-99 (molybdate) as tracer. J Lab Clin Med 62:330-340, 1963.

26. Patton DD: Rose bengal studies of the liver. In Continuing Education Lectures 1972, Southeastern Chapter of the Society of Nuclear Medicine, 1972, pp 5.1-5.14.

27. Jacksen RA, Bolles TF, Kubiatowicz DO, et al: Technetium-mercaptide complexes and their potential application as a liver specific agent. J Nucl Med 14:411-412, 1973.

28. Lin TH, Khentigan A, Winchell HS: A Tc-99m labeled replacement for I-131 rose bengal in liver and biliary tract studies. J Nucl Med 15:613-615, 1974.

29. Goris ML: I-123 iodobromsulphalein as a liver and biliary scanning agent. J Nucl Med 14:820-825, 1973.

30. Baker RJ, Bellen JC, Ronai PM: Technetium-99m - pyridoxylideneglutamate- a new hepatobiliary radiopharmaceutical. I. experimental aspects. J Nucl Med 16:720-727, 1975.

31. Ronai PM, Baker RJ, Bellen JC, et al: Technetium-99m - pyridoxylideneglutamate- a new hepatobiliary radiopharmaceutical. II. clinical aspects. J Nucl Med 16:728-737, 1975.

32. Birken S, Canfield RE: Labeled asialo-human chorionic gonadotropin as a liver scanning agent. J Nucl Med 15:1176-1178, 1974.

33. Harvey E, Loberg M, Cooper M: Tc-99m - HIDA- a new radiopharmaceutical for hepatobiliary imaging. J Nucl Med 16:533, 1975.

34. Kubota H, Poulose KP, Eckelman WC, et al: Technetium-99m pyridoxylideneglutamate- a new gallbladder scanning agent- comparative pharmacokinetic study with I-131 rose bengal. J Nucl Med 16:543, 1975.

35. Serafini AN, Smoak WM, Hupf HB, et al: Iodine-123-rose bengal- an improved hepatobiliary imaging agent. J Nucl Med 16:629-632, 1975.

36. Delprat GD: Studies on liver function-rose bengal elimination from the blood as influenced by liver injury. Acta Int Med 32:401-410, 1923.

37. Nordyke RA: Metabolic and physiologic aspects of I-131 rose bengal in studying liver function. In Seminars in Nuclear Medicine, Vol II (2), Freeman LM, Blaufox MD, Eds., New York, Grune & Stratton, Inc., 1972, pp 157-166.

38. Nordyke RA, Blahd WH: Blood disappearance of radioactive rose bengal-rapid simple test of liver function. JAMA 170:1159-1164, 1959.

39. Burke G, Halko A: Dynamic clinical studies with radioisotopes and the scintillation camera II rose bengal I-131 liver function studies. JAMA 198:140-150, 1966.

40. Wagner HN Jr, Miskin F: The liver. In Principles of Nuclear Medicine, Wagner HN Jr, Ed., Philadelphia, WB Saunders Company, 1968, pp 599-620.

41. Tubis M, Krishnamurthy GT, Endow JS, et al: Tc-99m penicillamine, a new cholescintigraphic agent. J Nucl Med 13:652-654, 1972.

42. Krishnamurthy GT, Endow JS, Tubis M, et al: Tc-99m penicillamine cholescintigraphy- comparison with oral cholecystography. J Nucl Med 14:418-419, 1973.

43. Waxman AD, Siemsen JK: Gallium gall bladder scanning in cholecystitis. J Nucl Med 16:148-150, 1975.

44. Fliegel CP, Dewanjee MK, Holman LB, et al: Tc-99m tetracycline as a kidney and gall bladder imaging agent. Radiology 110:407-412, 1973.

45. Schmidt U, Grafen P, Altland K, et al: Biochemistry and chemistry of lipoic acids. Advances in Enzymology 32:423-468, 1969.

46. Reed LJ: The chemistry and function of lipoic acid. Advances in Enzymology 18:319-346, 1957.

47. Koike M, Reed LJ, Carroll WR: α-keto acid dehydrogenation complexes I. purification and properties of pyruvate and α-ketoglutarate dehydrogenation complexes of Escherichia Coli. J Biol Chem 235:1924-1930, 1960.

48. Reed LJ, Cox DJ: Macromolecular organization of enzyme systems. Ann Rev Biochem 35:57-84, 1966.

49. Koike M, Reed LJ, Carroll WR: α-keto acid dehydrogenation complexes IV. resolution and reconstitution of the Escherichia Coli pyruvate dehydrogenation complex. J Biol Chem 238:30-39, 1963.

50. Hayakawa T, Hirashima MH, Ide S, et al: Isolation and properties of pyruvate and α-ketoglutarate dehydrogenation complexes from pig heart muscle. Biochem Biophys Commun 17:51, 1964.

51. Mukherjee BB, Matthews J, Horney DL, et al: Resolution and reconstitution of the E. Coli α-ketoglutarate dehydrogenase complex. J Biol Chem 240:PC2268-2269, 1965.

52. Hirashima M, Hawakaw T, Koike M: Mammalian α-keto acid dehydrogenation complexes. J Biol Chem 242:902-907, 1967.

53. Reed LJ: Oxidation of α-keto acids. J Vitaminology 14:77-85, 1968.

54. Reed LJ: Lipoic acid. In The Enzymes, 2nd ed, Vol 3, Boyer PD, Lardy H, Myrback K, Eds., New York, Academic Press, 1960, pp 195-223.

55. Bowles T: Personal communication. 3M Company, St. Paul, Minn., 1974.

56. Williams, ED, Glass HI, Arnot RN, et al: A dual detector scanner for quantitative uptake and organ volume studies. In Medical Radioisotope Scintigraphy, Vol 1, IAEA, Vienna, 1969, pp 665-683.

57. Sorenson, JA: Quantitative measurement of radioactivity in vivo by whole-body counting. In Instrumentation in Nuclear Medicine, Vol 2, Hine GJ, Sorenson JA Eds., New York, Academic Press, 1974, pp 311-318.

58. Sharma RR: Depth independence in quantitative radioisotope imaging. Br J Radiol 41:949, 1968.

59. Tothill P, Galt JM: Quantitative profile scanning for the measurement of organ radioactivity. Phys Med Biol 16:625-634, 1971.

60. Arimizu N, Morris AC: Quantitative measurement of radioactivity in internal organs by area scanning. J Nucl Med 10:265-269, 1969.

61. Bell PR, McClain WJ, Ross DA, et al: ORSS-72, A Computer-based Dual Data Rectilinear Scanning System. ORNL-TM-4045. Oak Ridge, 1973.

62. Bell PR, Dillon R: Personal communications. ORNL, Oak Ridge, 1975.

63. Mauderli W: Personal communications. University of Florida, Gainesville, Florida, 1974.

64. Sunderland ML: Radiochromatographic quality control- a simplified system. J Nucl Med 16:225-227, 1975.

65. Orvis AL: Assay of radiopharmaceuticals. In Instrumentation in Nuclear Medicine, Vol 2, Hine GJ, Sorenson JA, Eds., New York, Academic Press, 1974, pp 459-483.

66. Tipton IH: Specifications for standard man. In Radiological Health Handbook, Bureau of Radiological Health, Rockville, MD, USDHEW, 1970, pp 215-217.

67. McAfee JG: Problems in evaluating the radiation dose for radionuclides excreted by the kidneys. In Medical Radionuclides- Radiation Dose and Effects, Cloutier RJ, Edwards CL, Snyder WS, Eds., Oak Ridge, USAEC, 1970, pp 271-294.

68. Snyder WS, Ford MR, Warner GG, et al: Estimates of absorbed fractions for monoenergetic photon sources uniformly distributed in various organs of a homogenous phantom. MIRD Pamphlet No 5, J Nucl Med 10 (Suppl 3):5-52, 1969.

69. Butler PF, Fitzgerald LT, Vanek KN, et al: A computer program to determine cumulated activity and absorbed radiation dose. In Proceedings of the 1976 Radiopharmaceutical Dosimetry Symposium, Oak Ridge. To be published.

70. Butler PF: A Computer Program to Determine Cumulated Activity and Absorbed Radiation Dose. Master's thesis. University of Florida, 1976.

71. Loevinger R, Berman M: A schema for absorbed-dose calculations for biologically-distributed radionuclides. MIRD Pamphlet No 1, J Nucl Med (Suppl 1):7-14, 1968.

72. Smith EM: Calculating absorbed doses from radiopharmaceuticals. Nucleonics 24:33-39, 1966.

73. Smith EM, Brownell GL, Ellett WH: Radiation dosimetry. In Principles of Nuclear Medicine, Wagner HN Jr., Ed., Philadelphia, WB Saunders Company, 1968, pp 742-784.

74. Lathrop KA, Johnston RE, Blau M, et al: Radiation dose to humans from Se-75-L-selenomethionine. MIRD Pamphlet No 9, J Nucl Med (Suppl 6):7-30, 1972.

75. Snyder WS, Ford MR, Warner GG, et al: "S" Absorbed Dose Per Unit Cumulated Activity for Selected Radionuclides and Organs. MIRD Pamphlet 11, New York, Society of Nuclear Medicine, 1975.

76. Snyder WS, Ford MR, Watson SB: A Tabulation of Dose Equivalent Per Microcurie-day for Source and Target Organs of an Adult for Various Radionuclides. ORNL-5000, Oak Ridge, 1974.

77. Arimizu N, Morris AC Jr: Quantitative measurement of radioactivity in internal organs by area scanning. J Nucl Med 10:265-269, 1969.

78. Galt JM, Tothill P: The fate and dosimetry of two lung scanning agents, I-131-MAA and Tc-99m-ferrous hydroxide. Brit J Radiol 46: 272-276, 1973.

79. Morin RL, Brookeman VA: Yb-169-DTPA distribution and dosimetry in cisternography. J Nucl Med 15:786-796, 1974.

80. Williams ED, Merrick MV, Lavender JP: The distribution and dosimetry of In-111-bleomycin in man. Brit J Radiol 48:275-278, 1975.

81. Robbins PJ, Feller PA, Nishiyama H: Evaluation and dosimetry of a Tc-99m-Sn-MAA lung imaging agent in humans. Health Phys 30: 173-178, 1976.

82. Bernard SR, Hayes RL: Dose to various segments of the gastrointestinal tract. In Medical Radionuclides- Radiation Dose and Effects Cloutier RJ, Edwards CL, Snyder WS, Eds., Oak Ridge, USAEC, 1970, pp 295-314.

83. Skrable KW, Chabot G, Harris J, et al: Dosimetric model for the gastrointestinal tract. Health Phys 28:411-427, 1975.

84. MIRD Committee: Summary of current radiation dose estimates to humans from I-123, I-124, I-126, I-130, and I-131 as sodium rose bengal. MIRD dose estimate report No 7, J Nucl Med 16:1214-1217, 1975.

85. Guyton AC: Textbook of Medical Physiology, 3rd ed, Philadelphia, WB Saunders Company, 1967, pp 470-510.

86. Netter FH: The CIBA Collection of Medical Illustrations, Vol 6, CIBA, 1973, pp 2-67.

87. Hine GJ, Sorenson JA: Guide to the absorbed dose from internally administered radionuclides. In Instrumentation in Nuclear Medicine, Vol 2, Hine GJ, Sorenson JA, Eds., New York, Academic Press, 1974, pp 556-559.

88. Evans RD: Radium poisoning II. the quantitative determination of the radium content and radium elimination rate of living persons. Am J Roentgenol & Rad Therapy 37:368-378, 1937.

89. Hisada K, Ohba S, Matsudaira M: Isosensitive radioisotope scanning. Radiology 88:124-128, 1967.

90. Arimizu A, Kakehi H, Morris AC: Area scanning for quantitative measurement of radioactivity in internal organs. In Medical Radioisotope Scintigraphy, Vol 1, IAEA, Vienna, 1969, pp 653-663.

91. Tothill P, Galt JM: Quantitative profile scanning for the measurement of organ radioactivity. Phys Med Biol 16:625-634, 1971.

92. DuBois EF, DuBois D: Measurement of surface area of man. Arch Int Med 15:868, 1915.

93. DuBois EF, DuBois D: Formula to estimate approximate surface area if height and weight be known. Arch Int Med 17:863, 1916.

94. DeLand FH, North WA: Relationship between liver size and body size. Radiology 91:1195-1198, 1968.

BIOGRAPHICAL SKETCH

Kenneth Norman Vanek was born on October 22, 1945, in Chicago, Illinois. He graduated from Richardson High School in Richardson, Texas, in 1963. Mr. Vanek received the Bachelor of Science degree in zoology from Texas A & M University in 1967 and the Master of Science degree in biophysics in 1969.

In June, 1968, Mr. Vanek was commissioned in the United States Air Force and after receiving his master's degree, Lt. Vanek was sent to the Air Force Weapons Laboratory (AFWL) at Kirtland AFB, New Mexico, where he provided neutron dosimetry support to the Biophysics Division. After promotion to Captain in 1970, he was transferred within the AFWL to the Laser Division where he served as a management assistant to the Division Director.

From 1971 to 1973, Captain Vanek served as the health physicist and radiation protection officer at the Air Force Eastern Test Range [AFETR], Patrick AFB, Florida. He co-directed the Radiation Control Center during the launching of Pioneer F & G and served as the Air Force representative in the NASA Radiation Control Center during Apollo 16 and 17. Captain Vanek was also a member of the Interagency Nuclear Safety Review Panel for Viking and LES 8/9 [NASA, DOD, AEC]. Since 1973, Captain Vanek has been at the University of Florida pursuing a Doctor of Philosophy degree in medical radiation physics [Department of Nuclear Engineering Sciences] and upon graduation in 1976 will be assigned to the USAF Regional Hospital, Keesler AFB, Mississippi.

Professional society memberships include The Society of Nuclear Medicine, The Health Physics Society, The American Nuclear Society, The American Association of Physicists in Medicine, The International Radiation Protection Association, and The American Conference of Governmental Industrial Hygienists. He is also a member of the Tau Beta Pi national engineering honor society.

Captain Vanek is married to Sheila Ann Curry and has a son, Adam, and daughter, Tiffany.

I certify that I have read this study and that in my opinion it conforms to acceptable standards of scholarly presentation and is fully adequate, in scope and quality, as a dissertation for the degree of Doctor of Philosophy.

Valerie A. Brookeman, Chairperson
Associate Professor of Nuclear
Engineering Sciences

I certify that I have read this study and that in my opinion it conforms to acceptable standards of scholarly presentation and is fully adequate, in scope and quality, as a dissertation for the degree of Doctor of Philosophy.

Lawrence T. Fitzgerald
Assistant Professor of Radiology

I certify that I have read this study and that in my opinion it conforms to acceptable standards of scholarly presentation and is fully adequate, in scope and quality, as a dissertation for the degree of Doctor of Philosophy.

Genevieve S. Roessler
Assistant Professor of Nuclear
Engineering Sciences

I certify that I have read this study and that in my opinion it conforms to acceptable standards of scholarly presentation and is fully adequate, in scope and quality, as a dissertation for the degree of Doctor of Philosophy.

W. Emmett Bolch
Associate Professor of Nuclear
Engineering Sciences

I certify that I have read this study and that in my opinion it conforms to acceptable standards of scholarly presentation and is fully adequate, in scope and quality, as a dissertation for the degree of Doctor of Philosophy.

Mihran J. Ohanian
Professor of Nuclear Engineering Sciences

This dissertation was submitted to the Graduate Faculty of the College of Engineering and to the Graduate Council, and was accepted as a partial fulfillment of the requirements for the degree of Doctor of Philosophy.

August, 1976

Dean, College of Engineering

Dean, Graduate School